The BnamiR827–BnaA09.NLA1–BnaPHT1 module regulates phosphate homeostasis, pollen viability, and seed yield in Brassica napus

Article

Accepted Version

RESEARCH PAPER

The regulatory module *BnamiR827-BnaA09.NLA1-BnaPHT1s* modulates phosphate homeostasis, pollen viability and seed yield in *Brassica napus*

Running title:

BnamiR827-BnaNLA1 module regulates Pi homeostasis and seed yield in *B. napus*

Tao Wu[1,2], Bei Han[1,2], Yajie Wang[1,2], Bingbing Zhang[1,2], Chuang Wang[2], Sheliang Wang[1,2], Hongmei Cai[2], Zhu Liu[1], John P. Hammond[3], Surya Kant[4], Guangda Ding[1,2], Fangsen Xu[1,2], Lei Shi[1,2]*

[1] National Key Laboratory of Crop Genetic Improvement, Huazhong Agricultural University, Wuhan 430070, China

[2] Microelement Research Center, Key Laboratory of Arable Land Conservation (Middle and Lower Reaches of Yangtze River), Ministry of Agriculture and Rural Affairs, Huazhong Agricultural University, Wuhan 430070, China

[3] School of Agriculture, Policy and Development, University of Reading, Reading RG6 6AR, UK

[4] School of Agriculture, Biomedicine & Environment, La Trobe University, AgriBio, 5 Ring Rd, Bundoora, Vic 3083, Australia

*Correspondence: Lei Shi (leish@mail.hzau.edu.cn)

Address: National Key Laboratory of Crop Genetic Improvement, Huazhong Agricultural University, Wuhan 430070, China

Tel: 0086-27-87286871

Fax: 0086-27-87280016

Abstract

Phosphorus (P) is an essential macronutrient for the growth and yield of crops. However, there is limited understanding of the regulatory mechanisms of phosphate (Pi) homeostasis, and its impact on growth, development, and yield-related traits in *Brassica napus*. Here, we identified four *NITROGEN LIMITATION ADAPATATION1* (*BnaNLA1*) genes in *B. napus*, their expression was predominant in roots and suppressed by Pi starvation-induced *MicroRNA827s* (*BnamiR827s*). All the BnaNLA1 proteins have similar sequences, subcellular localizations, and abilities to rescue the growth defects of *atnla1* mutant. One of the genes, *BnaA09.NLA1* expressed abundantly in roots, and also in old leaves, anthers and pollens. Knocking out of *BnaNLA1*(s) or overexpressing *BnamiR827* resulted in increased concentrations of Pi in leaves as well as in stamen and had reduced pollen viability thereby negatively impacting seed yield. BiFC and split-ubiquitin Y2H analyses demonstrated that BnaA09.NLA1 interacted with seven Pi transporters highly expressed in roots and/or anthers (i.e., BnaPT8/10/11/27/35/37/42) to regulate Pi uptake and Pi allocation in anthers. Taken together, this study demonstrates that the *BnamiR827-BnaA09.NLA1-BnaPHT1s* module is involved in regulating Pi uptake and Pi allocation in floral organs, which is vital for the growth, pollen viability and seed yield of *B. napus*.

Keywords: *BnamiR827*, *BnaNLA1*, phosphate transporters, *Brassica napus*, pollen viability, seed yield

Highlight: The *BnamiR827-BnaA09.NLA1-BnaPHT1s* module is involved in regulating Pi uptake and Pi allocation in floral organs, which is vital for the growth, pollen viability and seed yield of *B. napus*.

Introduction

Phosphorus (P) is an indispensable macronutrient for plant growth and productivity. P is constituent of many macromolecules such as nucleic acids and phospholipids, and involved in numerous physiological processes including energy metabolism, signal transduction, photosynthesis, and respiration (White and Hammond, 2008). Plants acquire P in the form of inorganic phosphate (Pi), the concentration of which is often limited in the soil solution, since P is commonly present in organic and insoluble P forms (Raghothama and Karthikeyan, 2005; Lambers *et al*., 2008). The application of inorganic P fertilizers has greatly contributed to increment of yield and crop production (Syers *et al*., 2008). However, the excessive application of Pi fertilizers not only increases the cost of agricultural activities, but also leads to significant environmental problems, such as eutrophication and soil acidification (Zhang *et al*., 2013). Therefore, understanding how plants adapt to low and fluctuating soil Pi concentrations can facilitate crop breeding strategies to develop varieties with high P use efficiency, thus reducing the requirement for Pi fertilizers and contributing to sustainable agricultural practices.

Plants have evolved a series of adaptive strategies to improve Pi uptake and utilization efficiency (Wang *et al*., 2019). During short-term P starvation, intracellular Pi is maintained relatively constant at the cost of vacuolar Pi (Wang *et al*., 2015; Xu *et al*., 2019; Han *et al*., 2022). After the vacuolar Pi is exhausted, the plant cells synthetize and secrete acid phosphatases, ribonucleases and organic acids to liberate Pi fixed to soil minerals or present in organic forms, which are then taken up by root Pi transporters (Abel *et al*., 2000; Du *et al*., 2022; Liu *et al*., 2022). With a combination of high- and low-affinity Pi transporters, the Pi uptake system in plant roots operates over a broad range of Pi concentrations to optimize Pi uptake in this heterogeneous environment (Ai *et al*., 2009; Jia *et al*., 2011). Pi transporters (PHTs) have been divided into five families, i.e., PHT1, PHT2, PHT3, PHT4 and PHT5, playing key roles in Pi uptake, allocation and redistribution (Daram *et al*., 1999; Mudge *et al*., 2002; Guo *et al*., 2008; Liu *et al*., 2016; Versaw and Garcia, 2017).

PHT1;1 and PHT1;4 play major roles in Pi uptake, Pi uptake rate of the *pht1;1/pht1;4*

double mutant was reduced by 50% and 75% at low and high P concentration, respectively, compared with wild-type *Arabidopsis* (Shin *et al*., 2004; Catarecha *et al*., 2007). The expression of *PHT1;1* and *PHT1;4* was induced by P deficiency to enhance Pi uptake. Several mechanisms for *PHT1;1* and *PHT1;4* regulation have been reported. PHOSPHATE RESPONSEs (PHRs), WRKYs, and ABA INSENSITIVE5 (ABI5) acts as transcription factors (TFs) for *PHT1;1* (Nilsson *et al*., 2007; Wang *et al*., 2014; Su *et al*., 2015; Zhang *et al*., 2022a). In addition to transcriptional regulation, post-transcriptional modification controls the abundance and activity of PHT1 proteins. PHOSPHATE TRANSPORTER TRAFFIC FACILITATOR 1 (PHF1) is involved in the trafficking of PHT1s from the endoplasmic reticulum (ER) to the plasma membrane (PM), where they mediate Pi uptake (Gonzalez *et al*., 2005; Bayle *et al*., 2011; Guo *et al*., 2022). In rice, CASEIN KINASE2 (OsCK2) phosphorylates OsPT8 under P-sufficient conditions, and the phosphorylated OsPT8 cannot interact with OsPHF1, resulting in their retention in the ER (Chen *et al*., 2015). Whereas, under P-deficient conditions the protein PHOSPHATASE95 (OsPP95) dephosphorylates OsPT8, promoting its ER exit and trafficking to the PM (Yang *et al*., 2020). In addition, endosomal trafficking also regulates PHT1 abundance in the PM, where the cytosolic protein ALIX associates with the multivesicular bodies (MVB) by interacting with ESCRT-III subunit SNF7 and mediates PHT1;1 trafficking to the vacuole for degradation in *Arabidopsis* (Cardona-López et al 2015). Moreover, Sorting Nexin1 (SNX1) also plays a key role in the modulation of PHT1;1 protein stability and PM accumulation (Zhang *et al*., 2022b). The Rho of plant GTPase (AtROP6) acts as a molecular switch to modulate Pi uptake by inhibiting the activities of AtPHT1;1 and AtPHT1;4 in *Arabidopsis* (Gao *et al*., 2021). The RING-type ubiquitin ligase NITROGEN LIMITATION ADAPATATION1 (NLA1) and the ubiquitin-conjugating enzyme PHOSPHATE2 (PHO2) mediates the ubiquitination and degradation of PHT1 transporters in *Arabidopsis* and rice (Hu *et al*., 2011; Huang *et al*., 2013; Lin *et al*., 2013; Yue *et al*., 2017; Yang *et al*., 2020). *MicroRNA399* (*miR399*) suppresses the expression level of *PHO2* in *Arabidopsis*. However, *MicroRNA827* (*miR827*) targets *NLA1* and *OsSPX-MFS1* in *Arabidopsis* and rice, respectively (Pant *et al*., 2008; Hsieh

et al., 2009; Kant *et al*., 2011; Wang *et al*., 2012).

Besides being involved in Pi uptake, the *PHT1* family genes also play integral roles in Pi homeostasis in floral organs. Among the *OsPHT1* gene family, the transcript of *OsPHT1;7* was most abundant in anthers. In *Ospht1;7* mutants, anther development was significantly suppressed accompanied by a significant decrease in P concentration and inhibition of germination of pollen grains and pollen viability, leading to a reduction in seed-setting rate and grain yield (Dai *et al*., 2022). The *osnla1* mutant had reduced pollen fertility as well as impaired grain production. Also, the P concentration in the anther was higher in mutant revealing an association between P and pollen viability (Yang *et al*., 2020). OsPHT1;7 has been demonstrated to be a direct target of OsNLA1, with altered P concentrations in anthers and impaired pollen viability, indicating that P concentration in anthers need to be precisely maintained to ensure normal development of anthers and pollens (Yang *et al*., 2020; Dai *et al*., 2022).

Oilseed rape (*Brassica napus* L., genome $A_nA_nC_nC_n$) was formed about 7500 years ago by spontaneous hybridization between *Brassica rapa* (genome A_rA_r) and *Brassica oleracea* (genome C_oC_o), followed by chromosome doubling, a process known as allopolyploidy (Chalhoub *et al*., 2014). These polyploidy events led to numerous duplicated segments and homoeologous regions within the oilseed rape genome (Chalhoub *et al*., 2014). Thereby, a total of 49 *PHT1* genes have been identified in the genome of *B. napus*, namely *BnaPT1* to *BnaPT49* (Li *et al*., 2019), however, only *BnaPT11* and *BnaPT37* have been characterized. *BnaPT11* has been shown to be involved in Pi uptake, seed germination and early seedling growth in *B. napus* (Ren *et al*., 2014; Huang *et al*., 2019), while *BnaPT37* might be involved in Pi translocation from root to shoot and Pi distribution from source to sink (Li *et al*., 2023). Since *B. napus* is highly susceptible to P deficiency, it is important to understand the regulatory mechanisms of Pi uptake, transport and utilization in this allotetraploid crop.

Here, we report four *BnaNLA1* genes, expressed mainly in roots and are suppressed by P starvation and by miRNA; *BnamiR827*. All the BnaNLA1 proteins are homologs of *Arabidopsis* AtNLA1, and have similar sequences, subcellular localizations and abilities to rescue the growth defects of *nla1* mutation in *Arabidopsis*. BnaA09.NLA1

is shown to be involved in regulating Pi uptake, likely via degradation of several BnaPHT1 Pi transporters. Further, the *BnamiR827-BnaA09.NLA1* module is shown to be involved in pollen viability and seed production, a novel finding in dicotyledon species. A decline in pollen viability was due to an increase of Pi concentration in stamen, rather than in pistil. Importantly, *BnaA09.NLA1* and *BnaC08.NLA1* redundantly regulated Pi uptake, but *BnaA09.NLA1* played major roles in Pi allocation in anthers, suggests that a functional differentiation of *BnaNLA1* members evolved in *B. napus*. This work highlights the importance of the *BnamiR827-BnaA09.NLA1-BnaPHT1s* module in regulating Pi uptake in roots and Pi allocation in floral organs, which is vital for the growth, pollen viability and seed yield of *B. napus*.

Materials and methods

Plant materials and growth conditions

The *B. napus* cultivar 'Westar10' (W10) and *Arabidopsis thaliana* ecotype Columbia (Col-0) were used as wild-type in this study.

Nutrient solution experiments:

To evaluate whether *BnaNLA1s* are able to rescue the growth defects of the *Arabidopsis nla1* mutant, we grew Col-0, *nla1*, and *35S::BnaNLA1s* seedlings under a sufficient N supply (+N, 10 mM NO_3^-) and a deficient N supply (–N, 0.1 mM NO_3^-) for two weeks as previously described (Peng *et al*., 2007; Liu *et al*., 2017).

B. napus seeds were surface-sterilized and sown on moistened gauze, after 5 days of germination, uniform seedlings were transplanted and grown in black plastic containers filled with modified Hoagland solution. The seedlings were grown in a sufficient P supply (+P, 1 mM KH_2PO_4) for 8 days and then supplied with +P or a deficient P supply (-P, 5 μM KH_2PO_4) for a further 7 days to investigate seedling phenotypes and quantify gene expression. The full strength solution contained 5 mM KNO_3, 5 mM $Ca(NO_3)_2{\cdot}4H_2O$, 2 mM $MgSO_4{\cdot}7H_2O$, 50 μM EDTA-Fe (II), 0.32 μM $CuSO_4{\cdot}5H_2O$, 0.77 μM $ZnSO_4{\cdot}7H_2O$, 9.14 μM $MnCl_2{\cdot}4H_2O$ and 0.37 μM $Na_2MoO_4{\cdot}2H_2O$, pH 5.8. The P-sufficient solution (+P) contained 1 mM KH_2PO_4; the P-deficient solution (–P) contained 5 μM KH_2PO_4 and KCl was used to maintain K concentrations in the –P nutrient solution. All the plants were grown at 20 °C under a 16 hrs light/8 hrs dark

photoperiod with light intensity at 300-320 μmol m^{-2} s^{-1}, and the nutrient solution was replenished every 4 days.

Field trial and pot experiment:

The field trial and pot experiment were conducted at the experimental site of Huazhong Agricultural University in Wuhan (114.3° E, 30.5° N), Hubei Province, China from October 2022 to May 2023. The field soil is a yellow-brown (Alfisol) with pH 6.6, organic matter 10.70 g kg^{-1}, NH_4OAc-extracted potassium 120.20 mg kg^{-1}, available N (alkalihydrolysable N) 25.60 mg kg^{-1}, and P (Olsen-P) 8.30 mg kg^{-1}. The fertilizer application rates were: N 108 kg N ha^{-1} (supplied as urea, N ≥ 46%), P 90 kg P_2O_5 ha^{-1} (supplied as calcium superphosphate, P_2O_5≥ 12%), K 120 kg K_2O ha^{-1} (supplied as potassium chloride, K_2O ≥ 60%), and boron 15 kg ha^{-1} (supplied as $Na_2B_4O_7 \cdot 10H_2O$). These fertilizers were thoroughly mixed and applied in bands near the crop rows. For N, 60% was applied at initial basal stage and the remaining 40% N was top dressed during the overwintering stage.

The pot experiment was conducted at the farm with canopy of net screen. Two plants per pot (15 cm×20 cm) were grown, filled with 7 kg soil collected from the field. Each pot was supplied with 1,000 ml of nutrient solution containing 6.60 g $(NH_4)_2SO_4$, 2.01 g KH_2PO_4, 1.11 g KCl, 1.75 g $MgSO_4 \cdot 7H_2O$, 7 ml Arnon stock solution (1,000×) as micronutrient and 7 ml $FeSO_4$·EDTA Hogland stock solution (200×). Each pot received an additional 1 g of urea twice during the growth period. The Pi concentrations and pollen viability at the reproductive stage were measured, and the seed yield and yield related traits were measured at the maturity stage.

Vector construction and plant transformation

For the *BnaA09.NLA1/BnaC08.NLA1* CRISPR vector, a pair of target sequences sgRNA1 (GATCCGATATCATTAACCTGCGG) and sgRNA2 (TAGAGATCCTCCAATCACCATGG) were designed using CRISPR-P 2.0 (http://crispr.hzau.edu.cn) and then cloned into the CRISPR-Cas9 expression vector PKSE401 as per previously described method (Yang *et al*., 2017). To construct the overexpression vectors, the full-length coding sequences of *BnaNLA1s* and a DNA fragment (332 bp) including primary sequence of *BnamiR827* were amplified by PCR

and then cloned into the vector PBI121-GUS at the *Bam*H I and *Sac* I restriction sites driven by the CaMV35S promoter. To generate the GUS reporter vectors, the promoter sequences of *BnaA09.NLA1* (2160 bp), *BnaA09.miR827* (1556 bp), *BnaC08.miR827a* (1522 bp) and *BnaC08.miR827b* (1537 bp) were amplified by PCR from genomic DNA and then introduced into the DX2181b-GUS plasmid at the *Sma* I restriction site.

Transgenic *Arabidopsis* plants were produced using the previously reported 'floral dip' method (Clough and Bent 1998). All the *BnaNLA1s* overexpression vectors were delivered into *Arabidopsis nla1* mutant to generate complementary lines. The *proBnaA09.NLA1::GUS*, *proBnaA09.miR827::GUS, proBnaC08.miR827a::GUS* and *proBnaC08.miR827b::GUS* vectors were delivered into Col-0 background. The transformation of *B. napus* was performed using the hypocotyls of 'Westar10' by Agrobacterium infiltration (De Block *et al*., 1989) with *BnaA09.NLA1/BnaC08.NLA1* CRISPR vector, *BnamiR827* overexpression vector, and *proBnaA09.NLA1::GUS* vector. Positive transgenic plants were confirmed by PCR analysis. The T3 generation of homozygous *BnaNLA1* mutants, overexpression plants and GUS reporter lines were used for physiological and biochemical experimental analysis. The primer sequences used for cloning are listed in Table S1.

RNA isolation and RT-qPCR

Total RNA was extracted from plant tissues using an RNA isolation kit (Promega, Madison, WI, USA), then the first-strand cDNA was reverse transcribed by a cDNA synthesis kit (CWBIO, China). The real-time quantitative PCR (qRT-PCR) was carried out using a qRT-PCR master mix (SYBR® Premix Ex TaqTM II, Takara, Kyoto, Japan) with a real-time PCR detection system in Bio-Rad's ICYCleriQS fluorescent quantitative PCR instrument. The primer efficiency was assessed with Bio-Rad CFX Manager software (Bio-Rad, Hercules, CA, USA). The stem-loop reverse transcription PCR was used to quantify the mature *BnamiR827* according to the method by Chen *et al*. (2005), and the *BnaU6* small nuclear RNA (snRNA) was used as an internal control for each reaction (Cheng *et al*., 2017). The housekeeping genes *BnaTubulin* and *BnaEF1-α* were used as internal standards to normalize the expression level of *BnaNLA1s* genes. Three biological replicates and one plant per replicate were used for

gene expression analysis. The primer sequences used for qRT-PCR are shown in Table S1.

GUS histochemical analysis

Germinated *proBnaA09NLA1::GUS* transgenic *B. napus* seeds were grown in standard Hoagland nutrient solution for 10 days and then transferred to the nutrient solutions of 1 mM Pi (+P) or 5 μM Pi (-P) for 7 days. The *proBnaA09.miR827::GUS*, *proBnaC08.miR827a::GUS* and *proBnaC08.miR827b::GUS* transgenic plants were germinated on 1/2 MS medium for 5 days and then transplanted to medium with 625 μM Pi (+P) and 6.25 μM Pi (-P) for 3 days, respectively. Whole plants were submerged in GUS staining solution and incubated in the dark at 37℃ for 8 hrs. GUS histochemical staining was performed using a GUS staining kit (SL7160, Coolaber). After staining, the tissues were washed with 75% ethanol to remove chlorophyll and imaged using microscope (SMZ25, Nikon).

Subcellular localization and Biomolecular Fluorescence Complementation (BiFC)

For transient expression analysis of the subcellular localization of BnaNLA1 proteins in *Arabidopsis* protoplasts, the full-length coding sequence of each *BnaNLA1* genes were amplified from cDNA of 'Westar 10' and then cloned into the PM999-GFP vector driven by the CaMV35S promoter using the In-Fusion HD Cloning kit (Takara Bio). Transformation of *Arabidopsis* mesophyll protoplasts was performed according to Yoo *et al*. (2007). After 12-16 hrs incubation, the transformed protoplasts were imaged using confocal laser-scanning microscope (TCS SP8, Leica).

BnaA09.NLA1 gene was cloned into N-terminal fragments of YFP, and *BnaPHT1s* genes were cloned into C-terminal fragments of YFP vectors. The resulted constructs were transiently co-expressed in 4-week-old tobacco (*Nicotiana benthamiana*) leaves by Agrobacterium-mediated infiltration, as described previously (Walter *et al*., 2004). The YFP fluorescence signals in tobacco leaves were imaged 2 days after infiltration using confocal laser-scanning microscope (TCS SP8, Leica). Excitation/emission wavelengths were 488 nm/495–520 nm for GFP, 552 nm/575–630 nm for mCherry, and 514 nm/520–550 nm for YFP.

Split-ubiquitin yeast two-hybrid (Y2H) assay

The DUALmembrane Starter Kits (Dualsystems Biotech, Schlieren, Switzerland), was used for Y2H assays. The coding regions of seven BnaPHT1s and BnaA09.NLA1^{C275A} were cloned into vectors pBT3-N (containing the C terminal half of ubiquitin) and pPR3-N NubG (containing the mutated N-terminal half of ubiquitin), respectively. The primers used are listed in Table S1. The pNubG-Fe65 and pTSU2-APP plasmid combination was used as the positive control, while the pPR3-N and pBT3-N-BnaPHT1 plasmids were co-transformed into yeast cells as the negative controls and self-activation controls. Yeast strain NMY51 was co-transformed with the two constructs, and the transformed yeast cells were grown on SD (synthetic deficient)/-Leu-Trp (SD-LW), SD/-Leu-Trp-His (SD-LWH) and SD/-Leu-Trp-His-Ade (SD-LWHA) at 30°C for 3 days to test the protein interactions.

In vitro ubiquitination assay

In vitro ubiquitination assays were performed as described previously (Zhou *et al*. 2014). In brief, recombinant proteins AtUBA1-His, AtUBC8-His, MBP-AtNLA1, and MBP-AtNLA1^{C279A} were purified from *Escherichia coli*. 100 ng AtUBA1-His, 250 ng AtUBC8-His, 500 ng MBP-AtNLA1 (or MBP-AtNLA1^{C279A}), and 100 ng Flag-Ub (Boston Biochem) were mixed and incubated in 30 μL of a 1× ubiquitination reaction buffer (50 mM Tris-HCl pH 7.4, 5 mM $MgCl_2$, 2 mM ATP, 2 mM DTT, 0.1 mM $ZnSO_4$) at 30°C for 2 h. Samples were then heated to 95°C for 10 min before separation by SDS-PAGE and immunoblot analysis using anti-Flag antibody (Progeingene, 1:5000 dilution).

Measurement of Pi concentrations and total P concentrations

Tissue Pi concentrations were measured using the method described previously (Han *et al*., 2022). Briefly, 50 mg of fresh tissue samples were homogenized with 50 μl of 5 M H_2SO_4 and 1.5 ml of ddH_2O. After centrifugation at 12,000 *g* for 10 min at 4 °C, the supernatant was diluted and mixed with malachite green reagent (19.4 mM H_3BO_3, 27.64 mM $(NH_4)_6MO_7O_{24}.4H_2O$, 2.38 M H_2SO_4, 627.5 μM malachite green, and 0.1% polyvinyl alcohol) in a 3:1 ratio for 30 min. Then, 200 μL of the reaction mixture was taken to measure the absorbance at 650 nm using a microplate assay (Spark, Tecan, Switzerland). The Pi concentration was calculated based on a standard curve generated

using varying concentrations of KH_2PO_4.

For measurement of total P concentrations, 150 mg of dried and grounded plant tissue was pre-digested overnight in the glass tubes with concentrated sulfuric acid. The glass tubes were then heated to 120 °C and 4–5 drops of 30% H_2O_2 were added every 30 min until the solution turned colourless. After 30 min extension of heat digestion, total P concentrations were determined by molybdenum blue colorimetry at 700 nm using a microplate assay (Spark, Tecan, Switzerland).

Measurement of total chlorophyll concentrations

Leaf total chlorophyll was extracted with 80% acetone (v/v) at 4 °C for 24 hrs in darkness, and total chlorophyll per fresh weight was determined spectrophotometrically according to Arnon (1949).

Pollen viability assay

Pollen viability assay was performed as per previously reported method (Dai *et al*., 2022). Anthers were collected from five buds per branch, and three branches per plant were sampled one day before anthesis and submerged in 2% (w/v) I_2–KI solution for starch staining. Stained pollen grains were counted under microscope in bright field. Pollen viability was categorized into three groups: fertile with fully stained (black), partially stained (brown), and not stained (yellow or transparent). Three glass slides of each line and three fields of view of each glass slide were observed. In each field of view, no less than 100 pollen grains were assessed.

Accession numbers

Sequence data from this article can be found in the Arabidopsis Information Resource (TAIR, https://www.arabidopsis.org/) and the CNS-Genoscope genomic database (https://www.genoscope.cns.fr/brassicanapus/) under the following accession numbers: *AtNLA1* (At1g02860), *AtmiR827* (At3g59884), *BnaC05.NLA1* (BnaC05g01480D), *BnaA10.NLA1* (BnaA10g01450D), *BnaA09.NLA1* (BnaA09g51130D), *BnaC08.NLA1* (BnaC08g45940D), *BnaPT8* (BnaA04g22280D), *BnaPT10* (BnaA05g06210D), *BnaPT11* (BnaA05g06230D), *BnaPT27* (BnaA09g34510D), *BnaPT35* (BnaC04g06480D), *BnaPT37* (BnaC04g46050D) and *BnaPT42* (BnaC08g25460D).

Results

Identification and expression analysis of *BnaNLA1* genes in *B. napus*

To identify the *BnaNLA1* genes in *B. napus*, the *AtNLA1* gene sequence was used to perform a BLAST search in the genome of Westar10 (Song *et al*., 2020; 2021). A total of four homologs of *AtNLA1* were identified, namely, *BnaC05.NLA1*, *BnaC08.NLA1, BnaA09.NLA1* and *BnaA10.NLA1.* Gene structure analysis showed that each *BnaNLA1* genes had six exons, and the length of their encoding proteins varied from 330 to 333 amino acids, and all of them had a SPX domain and a RING domain (Supplementary Fig. S1, S2, S3). Phylogenetic analysis showed that four BnaNLA1 proteins were clustered into SPX-RING1 (NLA1) instead of SPX-RING2 (NLA2) subfamily, and they showed more than 83% identities and 88% similarities with their *Arabidopsis* homologs based on sequence alignments (Supplementary Fig. S1, S4).

To determine the expression patterns of *BnaNLA1s* in *B. napus* under different Pi availabilities, a time-course of transcript abundance was monitored using qRT-PCR. *BnaNLA1s* were expressed predominantly in roots and very less expression in leaves at the seedling stage in *B. napus* (Fig. 1A). Notably, *BnaNLA1s* were down-regulated in roots with increasing time after transfer to the low Pi availability, in contrast to leaves (Fig. 1A). The tissue-specific expression pattern of *BnaNLA1s* was determined at flowering time by qRT-PCR, showing that *BnaNLA1s* were still highly expressed in roots, compared to the different shoot tissues (Fig. 1B). In addition, *BnaC05.NLA1* and *BnaA10.NLA1* showed some notable expression in the root-shoot node, and *BnaA09.NLA1* in flowers (Fig. 1B).

To understand the details of tissue-specific expression, we generated transgenic *Arabidopsis* and *B. napus* lines expressing *proBnaA09.NLA1::GUS*. In *Arabidopsis*, GUS staining was observed in root epidermis, cortex, vascular bundle and root hairs at the four-leaf stage, while almost none was observed in leaves (Supplementary Fig. S5A-C). At the eight-leaf stage, *BnaA09.NLA1* was expressed mainly in roots, cotyledons and senile rosette leaves (Supplementary Fig. S5D). At the reproductive stage, *BnaA09.NLA1* was expressed mainly in roots, senescing rosette leaves, anthers and pollens (Supplementary Fig. S5E-K). In agreement with the qRT-PCR results and the GUS signal in transgenic *Arabidopsis*, *BnaA09.NLA1* was expressed strongly in *B.*

napus roots, including root epidermis, cortex and vascular bundle, and the overall expression was reduced after 7 days P starvation (Fig. 2A-E). In addition, expression of *BnaA09.NLA1* was also observed in cotyledons, the 1st leaf and the 2nd leaf, but the expression was not suppressed by P starvation (Fig. 2F, G). At the reproductive stage of *B. napus*, GUS staining was mainly observed in anthers, sepals and pollens (Fig. 2H, I). These data suggest that *BnaA09.NLA1* was involved in regulating cellular Pi status in multiple tissues, mainly in roots, old leaves, anthers and pollens.

Regulation of *BnaNLA1s* expression by phosphate-starvation-induced *miR827*

The *miR827* conservatively targets *PHT5* homologs in most angiosperms, but it preferentially targets *NLA1* homologs in *Brassicaceae* and *Cleomaceae* (Lin *et al*., 2018). Our previous results reported that there were no *miR827*-binding sites in the transcripts of *BnaPHT5;1*s (Han *et al*., 2022), suggesting they may target *BnaNLA1s*. To identify the *BnamiR827* genes in *B. napus*, the primary transcript sequence of *AtmiR827* was used to BLAST against the W10 genome. A total of three close homologs of *AtmiR827* were identified, namely, *BnaA09.miR827, BnaC08.miR827a* and *BnaC08.miR827b.* Although the primary transcript sequences of all these *BnamiR827* genes had several mismatched bases as per sequence alignments, their mature sequences were identical (Supplementary Fig. S6A). All three *BnamiR827* genes showed a typical "stem-loop" secondary structure according to the results predicted by RNAfold web server (Guber *et al*., 2008; Supplementary Fig. S6B), indicating that they were *miRNA* precursor genes. The *miR827*-binding site was then identified in the transcripts of *BnaNLA1s* and the results predicted by psRNATarget (http://plantgrn.noble.org/psRNATarget/) showed that all the *BnaNLA1s* possessed an effective *miR827*-binding site in their 5'-UTR (Supplementary Fig. S3).

To determine the expression patterns of *BnamiR827s* under different Pi availabilities, the transcript abundance of the precursor- and mature-*BnamiR827* were detected using qRT-PCR. Both the precursor- and mature-*BnamiR827* were significantly induced in roots and leaves following the transfer of plants to P-deficient conditions for seven days (Fig. 3A). The promoters of three *BnamiR827* genes were separated and transgenic *Arabidopsis* lines expressing *proBnaA09.miR827::GUS* (*pA09:GUS*),

proBnaC08.miR827a::GUS (*pC08a:GUS*) and *proBnaC08.miR827b::GUS* (*pC08b:GUS*) were generated. GUS staining results revealed that these three *BnamiR827* genes were significantly induced in both roots and leaves after three days of P starvation (Fig. 3B). At the reproductive stage, GUS stains of *proBnamiR827::GUS* transgenic *Arabidopsis* lines were observed in roots, rosette leaves, flowers, and siliques (Supplementary Fig. S7).

The expression of all *BnaNLA1s* was down-regulated, while the expression of *BnamiR827s* was up-regulated, in roots under P deficiency. Together with the location of *BnamiR827* binding sites in the 5'-UTR of the *BnaNLA1s* it suggests that *BnamiR827s* may directly suppress the expression of *BnaNLA1s* in *B. napus* roots in response to P deficiency. To determine this, transgenic *B. napus* lines overexpressing *BnaC08.miR827a* were constructed and the expression level of *BnamiR827*s and *BnaNLA1s* were quantified (Fig. 3C). The expression levels of all four *BnaNLA1s* were significantly decreased in the lines overexpressing *BnamiR827* (Fig. 3C). Consequently, we suggest that *BnaNLA1s* are down-regulated by *BnamiR827* in the roots of *B. napus* under P deficiency.

BnaNLA1s **functionally complement growth defects and early senescence of** ***Atnla1*** **under nitrogen deficient conditions**

BnaC05.NLA1, BnaA10.NLA1, BnaA09.NLA1 and BnaC08.NLA1 proteins shared 85.29%, 84.46%, 84.32% and 83.98% identities with AtNLA1 protein at the amino acid level, respectively (Supplementary Fig. S1). The high protein sequence identities between BnaNLA1s and AtNLA1 imply that BnaNLA1 proteins have PM localizations and ubiquitin E3 ligase activities like AtNLA1 and thus have similar functional properties. To validate the subcellular localizations of BnaNLA1 proteins, the coding sequences of BnaNLA1s were fused to C-terminus of GFP (GFP::BnaNLA1), and expressed transiently in *Arabidopsis* protoplasts using a PEG-mediated transformation system. GFP::BnaNLA1 proteins were detected mainly in the PM, merging with a PM marker AtPIP2a::mCherry. These results indicate that BnaNLA1s proteins were localized in PM (Fig. 4).

To examine conserved functionality of BnaNLA1s, we overexpressed four *BnaNLA1s*

in *Arabidopsis nla1* mutant background and observed their phenotypes under N sufficient (+N, 10 mM NO_3^-) and deficient (-N, 0.1 mM NO_3^-) conditions (Fig. 5). Under N sufficient conditions, all plants had comparable shoot fresh weight (SFW) and total chlorophyll concentrations, however, under N deficient conditions, *Arabidopsis nla1* mutant had significantly lower SFW and total chlorophyll concentrations compared to Col-0. While *35S::BnaNLA1s* lines had comparable SFW and total chlorophyll concentrations to Col-0 (Fig. 5A-C). This suggests that *BnaNLA1s* function similarly to rescue the growth defects and early senescence phenotype of the *Arabidopsis nla1* mutant under N deficient conditions.

The *BnamiR827-BnaA09.NLA1* module regulates Pi uptake in *B. napus*

Given that all the *BnaNLA1s* have high similarities in expression profiles, sequence identities, subcellular localizations and protein functions, we chose *BnaA09.NLA1*, and its closest homolog *BnaC08.NLA1*, to construct knock-out mutants using a CRISPR-Cas9 based gene editing system (Supplementary Fig. S8). First, we evaluated the effects of knocking out *BnaA09.NLA1* and *BnaC08.NLA1* double gene together (A09/C08-KOs) or *BnaA09.NLA1* alone (A09-KOs) on the growth performance of *B. napus* seedlings (Fig. 6A). A09-KO and A09/C08-KO lines had reduced shoot biomass compared to W10 under Pi sufficient conditions, but total root length did not show any significant differences between W10 and A09-KO, A09/C08-KO lines (Fig. 6B-C). Pi and total P concentrations were elevated in cotyledons or in leaves of A09-KO and A09/C08-KO lines compared to W10 under both P sufficient and P deficient conditions (Fig. 6D-G). Importantly, Pi and total P concentrations in cotyledons or in leaves of A09/C08-KO lines were higher than that of A09-KO lines (Fig. 6D-G), suggesting that *BnaA09.NLA1* and *BnaC08.NLA1* redundantly regulates Pi uptake in *B. napus.*

Considering that the transcript abundances of *BnaNLA1s* were down-regulated by overexpressing *BnamiR827* (Fig. 3C), we speculated that *BnamiR827* overexpressing lines (miR827-OEs) would phenocopy the A09-KO and A09/C08-KO lines. There were no significant differences in SFW or total root length between W10 and miR827-OE lines (Fig. 6I-J). Tissue Pi concentrations of the miR827-OE lines were significantly higher than those of W10 under P sufficient conditions (Fig. 6K), but only the Pi

concentrations in older leaves (L1 and L2) were significantly higher in miR827-OE lines than W10 under P deficient conditions (Fig. 6L). This suggests that *BnamiR827* affected P accumulation by suppressing the expression of *BnaNLA1s* in *B. napus*.

It has been reported that NLA1 regulates tissue Pi status in a nitrate-dependent manner in *Arabidopsis* (Kant *et al*., 2011), however, there were inconsistent results in rice (Yue *et al*., 2017; Zhong *et al*., 2017; Yang *et al*., 2020). To determine if *BnaA09.NLA1* regulates tissue Pi status in a nitrate-dependent or -independent manner, germinated seedlings were grown under sufficient Pi (1 mM) solution with three different concentrations of nitrate (10 mM, 1 mM and 0.1 mM). After 15 days, the cotyledon and 1st leaf were harvested for Pi analysis. Pi concentrations in the cotyledon and 1st leaf of W10 plants were significantly higher under low-nitrate supply (1 and 0.1 mM N) than under high N supply (10 mM N) (Supplementary Fig. S9). However, there were not significant differences of Pi concentrations in the cotyledon and 1st leaf of A09-KO, A09/C08-KO, and miR827-OE lines under different N supplies (Supplementary Fig. S9). Thus, *BnamiR827* and *BnaNLA1s* regulate tissue Pi status in a nitrate-independent manner at the seedling stage in *B. napus.*

The *BnamiR827-BnaA09.NLA1* module is involved in pollen development and seed yield

Since *BnaA09.NLA1* promoter was active in reproductive organs (Fig. 2H, I; Supplementary Fig. S4I, J), the role of *BnaA09.NLA1* in regulating tissue P status in floral organs and pollen development at flowering stage were further investigated. Pollen viability was assessed by the iodine staining method, with the intensity of pollen staining showed the presence of starch content in pollen, reflecting the pollen fertility (Fig. 7A). The W10 had 91% pollen fertility (fully stained), whereas decreased pollen fertility was observed in two independent lines in each A09-KO with 72% and 69%, A09/C08-KO with 69% and 74%, and miR827-OE with 58% and 56% (Fig. 7B). The W10 had 8% partially stained pollens, whereas, proportions for partially stained pollens was higher in A09-KO lines of 26% and 31%, A09/C08-KO lines of 30% and 26%, and miR827-OE lines of 39% and 39% (Fig. 7B). Moreover, the amount of sterile pollens (not stained) in miR827-OE lines was significantly higher compared to W10 plants, but

there was not significant difference in the amount of sterile pollen among W10, A09-KO, and A09/C08-KO lines (Fig. 7B).

In line with the impairment of pollen viability in A09-KO, A09/C08-KO, and miR827-OE lines, Pi concentrations in stamens (anthers) of these lines were higher than that of W10 plants (Fig. 7C). Additionally, petal and sepal Pi concentrations were higher in A09-KO, A09/C08-KO, and miR827-OE lines compared to W10 (Fig. 7C) though Pi concentrations in pistils were largely comparable between W10 plants and A09-KO, A09/C08-KO, and miR827-OE lines (Fig. 7C). These results indicate that the *BnamiR827-BnaA09.NLA1* module may regulate Pi status in stamens (anthers), which contributed to an impairment of pollen viability.

To investigate the growth performance and yield-related traits, W10, A09-KO, and A09/C08-KO lines were grown under field conditions and in pots under semi-controlled environment. Both A09-KO and A09/C08-KO lines had shorter plant height and lower shoot dry weight compared to W10 plants (Fig. 8A, C, D). There was significant decrease in branch number, pod number per plant, seed number per pod and seed yield in A09-KO, A09/C08-KO lines compared to W10 plants (Fig. 8B, F-I). Although there was no significant difference in 1000-seed weight between W10 plants and A09-KO, A09/C08-KO lines (Fig. 8J). Consistent with the field trial, an impairment in growth performance and a reduction in seed yield were also observed in the pot experiment, although there was no significant difference in plant height and branch numbers between W10 plants and A09-KO, A09/C08-KO lines (Supplementary Fig. S10).

In the field trial, overexpression of *BnamiR827* also led to a decrease in plant height, shoot dry weight, pod number per plant, seed number per pod and seed yield, but there was no significant difference in branch number and 1000-seed weight when compared to W10 plants (Fig. 8K-N, P-T). In addition, there was a significant increase in P concentration in the straw of miR827-OE lines when compared to W10 plants at harvest, which was also observed in A09/C08-KO2 line (Fig. 8E, O). These results indicate that the *BnamiR827-BnaA09.NLA1* module is required for the reproductive growth, pollen development, seed yield and yield-related traits in *B. napus*.

BnaA09.NLA1^{C275A} interacts with BnaPT8, BnaPT10, BnaPT11, BnaPT27, BnaPT35, BnaPT37 and BnaPT42

As in *Arabidopsis*, BnaA09.NLA1 might also regulate the protein levels of Pi transporters in *B. napus* because of the conservation of protein sequences and topologic structures between AtNLA1 and BnaNLA1s. To further determine which Pi transporters might be the potential targets of BnaA09.NLA1 in *B. napus*, we queried the BnIR (*Brassica napus* multi-omics information resource) database (Yang *et al*., 2023), and found that *BnaPT11*, *BnaPT17, BnaPT35* and *BnaPT37* had abundant expression in roots from the seedling stage to the flowering stage (Supplementary Fig. S11A). Moreover, *BnaPT8*, *BnaPT10*, *BnaPT11*, *BnaPT17*, *BnaPT35* and *BnaPT37* had abundant expression in anthers, and *BnaPT27* and *BnaPT42* were expressed specifically in anthers (Supplementary Fig. S11B). To examine whether these BnaPHT1s were direct targets of BnaA09.NLA1, the physical interactions between BnaA09.NLA1 and seven BnaPHT1 transporters were confirmed by BiFC assay in tobacco (*Nicotiana benthamiana*) leaves. These Pi transporters were chosen because of their predominate expression in roots and/or anthers (Supplementary Fig. S11), showing a co-expression with *BnaA09.NLA1* in the same tissues (Fig. 2; Supplementary Fig. S5).

When *BnaA09.NLA1* was co-expressed with the selected seven *BnaPHT1s*, no reconstituted yellow fluorescent protein (YFP) signals were observed (Fig. 9A). Then we mutated the conserved Cys (residue 275) to Ala (BnaA09.NLA1^{C275A}) in the RING domain of BnaA09.NLA1 protein and observed YFP signals in the PM resulting from the co-expression of *BnaA09.NLA1^{C275A}* with the seven *BnaPHT1s* (Fig. 9B). This interaction was specific because there was no YFP signal when *BnaA09.NLA1^{C275A}* or *BnaPHT1s* co-expressed with a PM-located boron transporter *NIP5;1* (Supplementary Fig. S12).

The last metal ligand residues are conserved between AtNLA1 (C279) and BnaA09.NLA1 (C275) (Supplementary Fig. S2). The *in vitro* ubiquitination assay revealed that mutation of C279 to A279 in AtNLA1 significantly decreased the E3 ubiquitin ligase activity (Fig. 9C). These results suggest that the compromise of

BnaA09.NLA1^{C275A} E3 ubiquitin ligase activity alleviates the degradation of BnaPHT1s in tobacco leaves. The split-ubiquitin Y2H assays were employed to retest the interactions between BnaA09.NLA1^{C275A} and BnaPHT1s. The NMY51 strain yeast cells co-expressing BnaA09.NLA1^{C275A} with BnaPHT1s were able to grow on the triple dropout medium (SD/−Leu/−Trp/−His, SD-LWH) and quadruple dropout medium (SD/−Leu/−Trp/−His/−Ade, SD-LWHA) (Fig. 9D), indicating that there were interactions between BnaA09.NLA1^{C275A} and BnaPHT1s. Taken together, our results reveal that seven BnaPHT1 family Pi transporters (i.e., BnaPT8, BnaPT10, BnaPT11, BnaPT27, BnaPT35, BnaPT37 and BnaPT42) are potential targets of BnaA09.NLA1 in *B. napus*.

Discussion

BnamiR827 regulates the expression of *BnaNLA1s* in response to Pi supply

Previous studies reported mechanisms regarding the Pi dependent regulation of *NLA1* expression in *Arabidopsis* and rice, i.e., *AtNLA1* expression is regulated by P deficiency induced by *AtmiR827*, while the expression of *OsNLA1* is controlled by upstream open reading frame (uORF)-mediated translational regulation (Kant *et al*., 2011; Yang *et al*., 2020). Here, we showed that all *BnaNLA1s* transcripts contain a *miR827*-binding site in their 5'-UTR (Supplementary Fig. S3). qRT-PCR analyses revealed that the expression of *BnaNLA1s* were down-regulated in roots with increasing expression of *BnamiR827* as Pi deficiency increased (Fig. 1A, 2A-E, 3A-B). Additionally, the expression of *BnaNLA1s* were repressed in roots of *BnamiR827* overexpression lines (Fig. 3C).

Shoot-derived *miR399* has been shown to function as a long-distance signal to suppress the expression of *PHO2* in roots (Chiang *et al*., 2023; Lin *et al*., 2008; Pant *et al*., 2008). The present study shows the induction of precursor-*BnamiR827* in roots priors to that in leaves after Pi deficiency (Fig. 3A), and stronger GUS signals in the roots of transgenic *Arabidopsis* than in leaves after 3 days of Pi starvation (Fig. 3B). These results revealed that mature-*BnamiR827* were derived from both roots and shoots to down-regulate the expression of *BnaNLA1s* under P deficiency in *B. napus*.

The Pi dependent expression of *AtNLA1s* in leaves is also regulated by *AtmiR827* in *Arabidopsis* (Lin *et al*., 2013). Although *BnamiR827* expression was also induced significantly by P deficiency in leaves, the expressions of *BnaNLA1s* in leaves were not

suppressed as in roots (Fig. 1A, 2F-G, 3A-B). Besides transcript cleavage, *AtmiR827* could regulate *AtNLA1* expression through translational repression (Liu *et al*., 2017). Further research is required to determine whether *miR827* regulates *NLA1* expression in *B. napus* roots by transcript cleavage, and in leaves by translational repression. Overall, our results suggest a different mechanism of *NLA1s* expression regulation in leaves between *Arabidopsis* and *B. napus*.

The *BnamiR827-BnaNLA1* module regulates Pi uptake in *B. napus*

The genome of *B. napus* has undergone complex polyploidization events, as a result, the members of many gene families have expanded (Chalhoub *et al*., 2014). For example, there are only nine *PHT1* Pi transporter family members in the *Arabidopsis* genome, while there are up to 49 members in the *B. napus* genome (Li *et al*., 2019). Here, we identified four *NLA1* members in *B. napus*, which exhibited similar gene expression patterns, subcellular localizations, and abilities to rescue the growth defects of *Arabidopsis nla1* mutant. Phenotype analysis revealed that Pi and P concentrations were elevated in cotyledons or leaves of A09-KO and A09/C08-KO lines (Fig. 6D-G). Notably, the P accumulation was higher in A09/C08-KO lines than in A09-KO lines, indicating the functional redundancy of *BnaNLA1* members in regulating Pi uptake (Fig. 6D-G).

It was the mutated version of *BnaA09.NLA1* (*BnaA09.NLA1*^{C275A}), but not the wild-type *BnaA09.NLA1*, that can reconstitute YFP signals when they are co-expressed with BnaPHT1s (Fig. 9), which suggests that the wild-type BnaA09.NLA1 might mediate the degradation of BnaPHT1s. Similar to *Arabidopsis*, rice, and soybean, BnaA09.NLA1 regulated Pi uptake by mediating the degradation of BnaPHT1 family members in roots (e.g., BnaPT11, BnaPT35 and BnaPT37) (Fig. 10), indicating that the mechanism of NLA1 in regulating Pi uptake among different species is conservative (Lin *et al*., 2013; Park *et al*., 2014; Yue *et al*., 2017; Du *et al*., 2020; Yang *et al*., 2020; Zhou *et al*., 2022).

It has been reported that *NLA1* regulates tissue Pi status in a nitrate-dependent manner in *Arabidopsis* (Kant *et al*., 2011), however, this observation is not consistent across species (Yue *et al*., 2017; Zhong *et al*., 2017; Yang *et al*., 2020). In this study, we found that there was no significant change in the cotyledon and 1st leaf Pi concentrations in the *BnaNLA1* mutants and *BnamiR827* overexpression lines when the external nitrate concentrations changed (Supplementary Fig. S9), indicating that the *BnaNLA1* mutants and *BnamiR827* overexpression lines take up Pi in a nitrate-independent manner at the

seedling stage. However, these differences could be due to species and plant growth stage specific, varying growing conditions and/or nitrate concentrations in growth media.

The *BnamiR827-BnaNLA1* module regulates pollen viability and seed yield in *B. napus*

Plant reproductive success requires a fine balance of nutrients, including P, to be available in the floral organs during pollen germination and fertilization (Luan *et al*., 2019; Dai *et al*., 2022). In *Arabidopsis*, Pi concentrations of floral organs including stamen, pistil, petal, and sepal were increased in the *vpt1/vpt3* mutant, with the excessive accumulation of Pi in the pistil leading to an impairment to reproductive growth (Luan *et al*., 2019). In contrast, P concentration in anther was significantly reduced in the rice *Ospht1;7* mutants, but significantly increased in anthers of the *Osnla1* mutants, both resulting in impaired pollen viability (Yang *et al*., 2020; Dai *et al*., 2022). In the current study, mutation of *BnaA09.NLA1* resulted in a disruption of tissue Pi concentrations in the floral organs, with an increase in Pi concentration in anthers, resulting in a reduction in pollen viability (Fig. 7). The *BnaA09.NLA1*/*BnaC08.NLA1* double gene mutants had a significantly low pollen viability compared to W10, however it was comparable to the *BnaA09.NLA1* mutants (Fig. 7), indicating that *BnaA09.NLA1* might play major role in maintaining tissue Pi concentrations in the floral organs. There was no significant difference of Pi concentrations in the pistil among W10 plants, A09-KO, A09/C08-KO and miR827-OE lines, except one of A09/C08-KO lines (Fig. 7C). These results and the evident expression of *BnaA09.NLA1* in anthers and pollens (Fig. 2H, 2I) suggest that *BnaA09.NLA1* regulates the male floral tissue Pi concentrations, which is different from the *VPT* genes (Luan *et al*., 2019).

Transcriptome data showed that within the entire *BnaPHT1* family, *BnaPT8*, *BnaPT10*, *BnaPT11*, *BnaPT17*, *BnaPT35* and *BnaPT37* were expressed abundantly in anthers, and *BnaPT27* and *BnaPT42* were expressed specifically in anthers (Supplementary Fig. S11B). The BiFC and Y2H analyses had validated seven BnaPHT1s (i.e., BnaPT8, BnaPT10, BnaPT11, BnaPT27, BnaPT35, BnaPT37 and BnaPT42) as potential targets

of BnaA09.NLA1 (Fig. 9), suggesting that BnaA09.NLA1 acts on these BnaPHT1 members to regulate Pi allocation in male floral organs and pollen viability.

Improving the Pi uptake efficiency of crops is an effective strategy to enhance crops yield. Overexpression of *TaPHR1-A1* or *TaPHR3-A1* genes promotes Pi uptake and increases grain yield mainly by improving grain number in wheat (Wang *et al*., 2013; Zheng *et al*., 2020). Mutation of *TaPHO2-A*, one homologous gene of *TaPHO2* members in wheat, increases Pi uptake efficiency and results in 14%-17% increase of wheat yield (Ou *et al*., 2016). In soybean, yield positively correlates with Pi absorption capacity, and *GmPHF1* was identified as a locus to improve Pi absorption and yield (Guo *et al*., 2022).

In this study, we aimed to improve plant Pi uptake efficiency by knocking out some copies of *BnaNLA1s* (this cannot be achieved in rice because only one *NLA1* gene existed), thereby increasing seed yield of *B. napus*. Unexpectedly, both *BnaA09.NLA1* and *BnaA09.NLA1/BnaC08.NLA1* mutants showed sharp decreases in pollen viability and thereby reduced seed yield (Fig. 7, 8; Supplementary Fig. S10). These results highlight the importance of tissue specific Pi status in maintaining reproductive performance and ultimately seed yield in *B. napus*. Therefore, we should evaluate the potential effects particularly on the Pi concentrations in the floral organs and pollen viability when a key future genetic locus for consideration in improving Pi uptake and utilization efficiency and seed yield in crops. Applying CRISPR/Cas9 system to edit the promoter (Li *et al*., 2020) to knock down the expression of *BnaA09.NLA1* in the root without changing its expression in anthers is a possible strategy to improve Pi uptake efficiency and seed yield of *B. napus*. Given that mutation of *BnaC08.NLA1* in the A09-KO background further increases the P concentrations in shoots of *B. napus* but had lesser impact on the pollen viability and seed yield (Fig. 6-8), whether *BnaC08.NLA1* can be used as a target to improve Pi uptake efficiency of *B. napus* should be investigated in the future.

Here, we propose a functional model (Fig. 10) that P deficiency induces *BnamiR827* to regulate the expression of *BnaNLA1s* at a post-transcriptional level, and BnaA09.NLA1 mediates the degradation of several BnaPHT1s (i.e., BnaPT8, BnaPT10, BnaPT11,

BnaPT27, BnaPT35, BnaPT37 and BnaPT42) to regulate Pi uptake and homeostasis in anthers, pollen viability, and effect on seed yield in *B. napus*.

Supplementary data

The following supplementary data are available at *JXB* online.

Fig. S1 Visualization of domains, and the sequence identity and similarity among NLA1 proteins.

Fig. S2 Sequence alignment of AtNLA1 and BnaNLA1 proteins.

Fig. S3 Gene structures of *NLA1s* and their *miR827* binding site in *Arabidopsis* and *B. napus*.

Fig. S4 The phylogenetic tree of the SPX-RING proteins in different species.

Fig. S5 Tissue-specific expression pattern of *BnaA09.NLA1* in transgenic *Arabidopsis* in different plant organs.

Fig. S6 Sequence alignment of primary transcript and the secondary structure of *BnamiR827s*.

Fig. S7 Tissue-specific expression patterns of *BnamiR827* genes in transgenic *Arabidopsis* in different plant organs.

Fig. S8 The mutation types of (A) *BnaA09.NLA1* knockout lines and (B) *BnaA09.NLA1/BnaC08.NLA1* knockout lines generated by the CRISPR-Cas9 system.

Fig. S9 Mutation of *BnaA09.NLA1/BnaC08.NLA1* and overexpression of *BnamiR827* increase the P accumulation at different nitrate concentrations.

Fig. S10 Growth performance and yield related traits of W10, A09-KO and A09/C08-KO lines in the pot experiments.

Fig. S11 Expression profiles of the *BnaPHT1* family genes under sufficient P supply.

Fig. S12 Interaction of nYFP-BnaA09.NLA1 or nYFP-BnaA09.NLA1^{C275A} with NIP5;1-cYFP, cYFP-BnaPHT1s with NIP5;1-nYFP, and NIP5;1-nYFP with NIP5;1-cYFP in BiFC assay.

Table S1 Primers used in this study.

Acknowledgments

We thank Prof. Steven J. Rothstein (Department of Molecular and Cellular Biology, University of Guelph, Canada) for kindly providing the *Arabidopsis nla1* mutant seeds, and Prof. Wenxue Li (National Key Facility for Crop Gene Resources and Genetic Improvement, Institute of Crop Science, Chinese Academy of Agricultural Sciences, China) for his help in sending the mutant seeds.

Author contributions

Lei Shi and Tao Wu planned and designed the research. Tao Wu performed experiments, Bei Han, Yajie Wang and Bingbing Zhang helped in constructing the genetic materials, or performing physiological experiments. Tao Wu and Lei Shi analyzed the data and drafted the manuscript. Chuang Wang, Sheliang Wang, Hongmei Cai, Zhu Liu, John P. Hammond, Surya Kant, Guangda Ding and Fangsen Xu gave critical comments during study and revisions of the manuscript. Lei Shi agrees to serve as the author responsible for contact and ensuring communication.

Conflict of interest

The authors declare no conflict of interest.

Funding

This work was supported by the STI 2030－Major Project （2023ZD04072) and National Nature Science Foundation of China (Grants No. 32172662 and 31972498).

Data availability

The data supporting the findings of this study are available within the manuscript and within its supplementary data published online.

References

Abel S, Nürnberger T, Ahnert V, Krauss GJ, Glund K. 2000. Induction of an extracellular cyclic nucleotide phosphodiesterase as an accessory ribonucleolytic

activity during phosphate starvation of cultured tomato cells. Plant Physiology **122**, 543–552.

Ai P, Sun S, Zhao J, Fan X, Xin W, Guo Q, Yu L, Shen Q, Wu P, Miller AJ, *et al.* 2009. Two rice phosphate transporters, OsPht1;2 and OsPht1;6, have different functions and kinetic properties in uptake and translocation. The Plant Journal **57**, 798-809.

Arnon DI. 1949. Copper enzymes in isolated chloroplasts. Polyphenoloxidase in *Beta vulgaris*. Plant Physiology **24**, 1–15.

Bayle V, Arrighi J-F, Creff A, Nespoulous C, Vialaret J, Rossignol M, Gonzalez E, Paz-Ares J, Nussaume L. 2011. Arabidopsis thaliana high-affinity phosphate transporters exhibit multiple levels of posttranslational regulation. The Plant Cell **23**, 1523–1535.

Cardona-López X, Cuyas L, Marín E, Rajulu C, Irigoyen ML, Gil E, Puga MI, Bligny R, Nussaume L, Geldner N, *et al.* 2015. ESCRT-III-associated protein ALIX mediates high-affinity phosphate transporter trafficking to maintain phosphate homeostasis in Arabidopsis. The Plant Cell **27**, 2560–2581.

Catarecha P, Segura MD, Franco-Zorrilla JM, García-Ponce B, Lanza M, Solano R, Paz-Ares J, Leyva A. 2007. A mutant of the Arabidopsis phosphate transporter PHT1;1 displays enhanced arsenic accumulation. The Plant Cell **19**, 1123–1133.

Chalhoub, B, Denoeud, F, Liu, S, Parkin, IA, Tang, H, Wang, X, *et al.* 2014. Early allopolyploid evolution in the post-neolithic *Brassica napus* oilseed genome. Science **345**, 950–953.

Chen C, Ridzon DA, Broomer AJ, Zhou Z, Lee DH, Nguyen JT, *et al.* 2005. Real-time quantification of microRNAs by stem-loop RT-PCR. Nucleic Acids Research **33**: e179.

Chen J, Wang Y, Wang F, Yang J, Gao M, Li C, Liu Y, Liu Y, Yamaji N, Ma JF, *et al.* 2015. The rice CK2 kinase regulates trafficking of phosphate transporters in response to phosphate levels. The Plant Cell **27**, 711–723.

Cheng H, Hao M, Wang W, Mei D, Wells R, Liu J, *et al*. 2017. Integrative RNA- and miRNA-profile analysis reveals a likely role of BR and auxin signaling in branch angle regulation of *B. napus*. International Journal of Molecular Sciences **18**: 887.

Chiang CP, Li JL, Chiou TJ. 2023. Dose-dependent long-distance movement of microRNA399 duplex regulates phosphate homeostasis in Arabidopsis. New Phytologist **240**, 802–814.

Clough SJ, Bent AF. 1998. Floral dip: a simplified method for Agrobacterium-mediated transformation of *Arabidopsis thaliana*. The Plant Journal **16**, 735–743.

Dai C, Dai X, Qu H, Men Q, Liu J, Yu L, Gu M, Xu G. 2022. The rice phosphate transporter OsPHT1;7 plays a dual role in phosphorus redistribution and anther development. Plant Physiology **188**, 2272–2288.

Daram P, Brunner S, Rausch C, Steiner C, Amrhein N, Bucher M. 1999. Pht2;1 encodes a low-affinity phosphate transporter from Arabidopsis. The Plant Cell **11**, 2153–2166.

De Block M, De Brouwer D, Tenning P. 1989. Transformation of *Brassica napus* and *Brassica oleracea* using Agrobacterium tumefaciens and the expression of the bar and neo genes in the transgenic plants. Plant Physiology **91**, 694–701.

Du W, Ning L, Liu Y, Zhang S, Yang Y, Wang Q, Chao S, Yang H, Huang F, Cheng H, *et al*. 2020. Identification of loci and candidate gene *GmSPX-RING1* responsible for phosphorus efficiency in soybean via genome-wide association analysis. BMC Genomics **21**, 725.

Du Z, Deng S, Wu Z, Cai H, Xu F, Shi L, Wang S, Ding G, Wang C. 2022. Characterization of the PHOSPHATE RESPONSE 2-dependent and -independent Pi-starvation response secretome in rice. Journal of Experimental Botany **73**, 6955–6970.

Gao H, Wang T, Zhang Y, Li L, Wang C, Guo S, Zhang T, Wang C. 2021. GTPase ROP6 negatively modulates phosphate deficiency through inhibition of PHT1;1 and PHT1;4 in Arabidopsis thaliana. Journal of Integrative Plant Biology **63**, 1775–1786.

González E, Solano R, Rubio V, Leyva A, Paz-Ares J. 2005. PHOSPHATE

776 TRANSPORTER TRAFFIC FACILITATOR1 is a plant-specific SEC12-related
777 protein that enables the endoplasmic reticulum exit of a high-affinity phosphate
778 transporter in Arabidopsis. The Plant Cell **17**, 3500–3512.
779 **Gruber AR, Lorenz R, Bernhart SH, Neubock R, Hofacker IL.** 2008. The vienna
780 RNA websuite. Nucleic Acids Research **36**, W70–W74.
781 **Guo B, Jin Y, Wussler C, Blancaflor EB, Motes CM, Versaw WK.** 2007. Functional
782 analysis of the Arabidopsis PHT4 family of intracellular phosphate transporters.
783 New Phytologist **177**, 889–898.
784 **Guo Z, Cao H, Zhao J, Bai S, Peng W, Li J, Sun L, Chen L, Lin Z, Shi C, *et al*.**
785 2022. A natural uORF variant confers phosphorus acquisition diversity in soybean.
786 Nature Communications **13**, 3796.
787 **Han B, Wang C, Wu T, Yan J, Jiang A, Liu Y, Luo Y, Cai H, Ding G, Dong X, *et al*.**
788 2022. Identification of vacuolar phosphate influx transporters in *Brassica napus*.
789 Plant, Cell & Environment **45**, 3338–3353.
790 **Hsieh LC, Lin SI, Shih AC, Chen JW, Lin WY, Tseng CY, Li WH, Chiou TJ.** 2009
791 Uncovering small RNA-mediated responses to phosphate deficiency in
792 Arabidopsis by deep sequencing. Plant Physiology **151**, 2120-2132.
793 **Hu B, Zhu C, Li F, Tang J, Wang Y, Lin A, Liu L, Che R, Chu C.** 2011. LEAF TIP
794 NECROSIS1 plays a pivotal role in the regulation of multiple phosphate starvation
795 responses in rice. Plant Physiology **156**, 1101–1115.
796 **Huang KL, Wang H, Wei YL, Jia HX, Zha L, Zheng Y, Ren F, Li XB.** 2019. The
797 high-affinity transporter BnPHT1;4 is involved in phosphorus acquisition and
798 mobilization for facilitating seed germination and early seedling growth of
799 *Brassica napus*. BMC Plant Biology **19**, 156.
800 **Huang TK, Han CL, Lin SI, Chen YJ, Tsai YC, Chen YR, Chen JW, Lin WY, Chen**
801 **PM, Liu TY, *et al*.** 2013. Identification of downstream components of ubiquitin-
802 conjugating enzyme PHOSPHATE2 by quantitative membrane proteomics in
803 Arabidopsis roots. The Plant Cell **25**, 4044–4060.
804 **Jia H, Ren H, Gu M, Zhao J, Sun S, Zhang X, Chen J, Wu P, Xu G.** 2011. The
805 phosphate transporter gene OsPht1;8 is involved in phosphate homeostasis in rice.

Plant Physiology **156**, 1164–1175.

Kant S, Peng M, Rothstein SJ. 2011. Genetic regulation by NLA and microRNA827 for maintaining nitrate-dependent phosphate homeostasis in Arabidopsis. PLoS Genetics **7**, e1002021.

Lambers H, Raven J, Shaver G, Smith S. 2008. Plant nutrient-acquisition strategies change with soil age. Trends in Ecology & Evolution **23**, 95–103.

Li C, Li W, Zhou Z, Chen H, Xie C, Lin Y. 2020. A new rice breeding method: CRISPR/Cas9 system editing of the *Xa13* promoter to cultivate transgene-free bacterial blight-resistant rice. Plant Biotechnology Journal **18**, 313–315.

Li Y, Wang X, Zhang H, Wang S, Ye X, Shi L, Xu F, Ding G. 2019. Molecular identification of the phosphate transporter family 1 (PHT1) genes and their expression profiles in response to phosphorus deprivation and other abiotic stresses in *Brassica napus*. PLoS One **14**, e0220374.

Li Y, Wang X, Zhang H, Ye X, Shi L, Xu F, Ding G. 2023. Phosphate transporter *BnaPT37* regulates phosphate homeostasis in *Brassica napus* by changing its translocation and distribution in vivo. Plants (Basel) **12**, 3362.

Lin SI, Chiang SF, Lin WY, Chen JW, Tseng CY, Wu PC, Chiou TJ. 2008. Regulatory network of microRNA399 and PHO2 by systemic signaling. Plant Physiology **147**, 732–746.

Lin WY, Huang TK, Chiou TJ. 2013. Nitrogen limitation adaptation, a target of microRNA827, mediates degradation of plasma membrane-localized phosphate transporters to maintain phosphate homeostasis in Arabidopsis. The Plant Cell **25**, 4061–4074.

Lin WY, Lin YY, Chiang SF, Syu C, Hsieh LC, Chiou TJ. 2018. Evolution of microRNA827 targeting in the plant kingdom. New Phytologist **217**, 1712–1725.

Liu T, Deng S, Zhang C, Yang X, Shi L, Xu F, Wang S, Wang C. 2023. Brassinosteroid signaling regulates phosphate starvation-induced malate secretion in plants. Journal of Integrative Plant Biology **65**, 1099–1112.

Liu TY, Huang TK, Yang SY, Hong YT, Huang SM, Wang FN, Chiang SF, Tsai SY, Lu WC, Chiou TJ. 2016. Identification of plant vacuolar transporters mediating

phosphate storage. Nature Communications **7**, 11095.

Liu W, Sun Q, Wang K, Du Q, Li WX. 2017. Nitrogen Limitation Adaptation (NLA) is involved in source-to-sink remobilization of nitrate by mediating the degradation of NRT1.7 in *Arabidopsis*. New Phytologist **214**, 734–744.

Luan M, Zhao F, Han X, Sun G, Yang Y, Liu J, Shi J, Fu A, Lan W, Luan S. 2019. Vacuolar phosphate transporters contribute to systemic phosphate homeostasis vital for reproductive development in Arabidopsis. Plant Physiology **179**, 640–655.

Mudge SR, Rae AL, Diatloff E, Smith FW. 2002. Expression analysis suggests novel roles for members of the Pht1 family of phosphate transporters in Arabidopsis. The Plant Journal **31**, 341–353.

Nilsson L, Müller R, Nielsen TH. 2007. Increased expression of the MYB-related transcription factor, PHR1, leads to enhanced phosphate uptake in Arabidopsis thaliana. Plant, Cell & Environment **30**, 1499–1512.

Ouyang X, Hong X, Zhao X, Zhang W, He X, Ma W, Teng W, Tong Y. 2016. Knock out of the *PHOSPHATE 2* gene *TaPHO2-A1* improves phosphorus uptake and grain yield under low phosphorus conditions in common wheat. Scientific Reports **6**, 29850.

Pant BD, Buhtz A, Kehr J, Scheible WR. 2008. MicroRNA399 is a long-distance signal for the regulation of plant phosphate homeostasis. The Plant Journal **53**, 731–738.

Park BS, Seo JS, Chua NH. 2014. NITROGEN LIMITATION ADAPTATION recruits PHOSPHATE2 to target the phosphate transporter PT2 for degradation during the regulation of Arabidopsis phosphate homeostasis. The Plant Cell **26**, 454–464.

Peng M, Hannam C, Gu H, Bi YM, Rothstein SJ. 2007. A mutation in *NLA*, which encodes a RING-type ubiquitin ligase, disrupts the adaptability of *Arabidopsis* to nitrogen limitation. The Plant Journal **50**, 320–337.

Raghothama KG, Karthikeyan AS. 2005. Phosphate acquisition. Plant and Soil **274**, 37–49.

Ren F, Zhao CZ, Liu CS, Huang KL, Guo QQ, Chang LL, Xiong H, Li XB. 2014.

A *Brassica napus* PHT1 phosphate transporter, BnPht1;4, promotes phosphate uptake and affects roots architecture of transgenic Arabidopsis. Plant Molecular Biology **86**, 595–607.

Shin H, Shin HS, Dewbre GR, Harrison MJ. 2004. Phosphate transport in Arabidopsis: Pht1;1 and Pht1;4 play a major role in phosphate acquisition from both low- and high-phosphate environments. The Plant Journal **39**, 629–642.

Song JM, Guan Z, Hu J, Guo C, Yang Z, Wang S, Liu D, Wang B, Lu S, Zhou R, *et al*. 2020. Eight high-quality genomes reveal pan-genome architecture and ecotype differentiation of *Brassica napus*. Nature Plants **6**, 34–45.

Song JM, Liu DX, Xie WZ, Yang Z, Guo L, Liu K, Yang QY, Chen LL. 2020. BnPIR: Brassica napus pan-genome information resource for 1689 accessions. Plant Biotechnology Journal **19**, 412–414.

Su T, Xu Q, Zhang FC, Chen Y, Li LQ, Wu WH, Chen YF. 2015. WRKY42 modulates phosphate homeostasis through regulating phosphate translocation and acquisition in Arabidopsis. Plant Physiology **167**, 1579–1591.

Syers JK, Johnston AE, Curtin D. 2008. Effciency of soil and fertilizer phosphorus use: reconciling changing concepts of soil phosphorus behaviour with agronomic information. FAO, Rome.

Versaw WK, Garcia LR. 2017. Intracellular transport and compartmentation of phosphate in plants. Current Opinion in Plant Biology **39**, 25–30.

Walter M, Chaban C, Schütze K, Batistic O, Weckermann K, Näke C, Blazevic D, Grefen C, Schumacher K, Oecking C, Harter K, Kudla J. 2004. Visualization of protein interactions in living plant cells using bimolecular fluorescence complementation. The Plant Journal **40**, 428–438.

Wang C, Huang W, Ying Y, Li S, Secco D, Tyerman S, Whelan J, Shou H. 2012. Functional characterization of the rice *SPX-MFS* family reveals a key role of *OsSPX-MFS1* in controlling phosphate homeostasis in leaves. New Phytologist **196**, 139–148.

Wang C, Yue W, Ying Y, Wang S, Secco D, Liu Y, Whelan J, Tyerman SD, Shou H. 2015. Rice SPX-major facility superfamily3, a vacuolar phosphate efflux

transporter, is involved in maintaining phosphate homeostasis in rice. Plant Physiology **169**, 2822–2831.

Wang H, Xu Q, Kong YH, Chen Y, Duan JY, Wu WH, Chen YF. 2014. Arabidopsis WRKY45 transcription factor activates *PHOSPHATE TRANSPORTER1;1* expression in response to phosphate starvation. Plant Physiology **164**, 2020–2029.

Wang J, Sun J, Miao J, Guo J, Shi Z, He M, Chen Y, Zhao X, Li B, Han F, *et al*. 2013. A phosphate starvation response regulator Ta-PHR1 is involved in phosphate signalling and increases grain yield in wheat. Annals of Botany **111**, 1139–1153.

Wang W, Ding G, White PJ, Wang X, Jin K, Xu F, Shi L. 2019. Mapping and cloning of quantitative trait loci for phosphorus efficiency in crops: opportunities and challenges. Plant and Soil **439**, 91–112.

White PJ, Hammond JP. 2008. Phosphorus nutrition of terrestrial plants. In: The Ecophysiology of Plant-Phosphorus Interactions. Plant Ecophysiology **7**, 51–81.

Xu L, Zhao H, Wan R, Liu Y, Xu Z, Tian W, Ruan W, Wang F, Deng M, Wang J, *et al*. 2019. Identification of vacuolar phosphate efflux transporters in land plants. Nature Plants **5**, 84–94.

Yang H, Wu JJ, Tang T, Liu KD, Dai C. 2017. CRISPR/Cas9-mediated genome editing efficiently creates specific mutations at multiple loci using one sgRNA in *Brassica napus*. Scientific Reports **7**, 7489.

Yang SY, Lu WC, Ko SS, Sun CM, Hung JC, Chiou TJ. 2020. Upstream open reading frame and phosphate-regulated expression of rice *OsNLA1* controls phosphate transport and reproduction. Plant Physiology **182**, 393–407.

Yang Z, Wang S, Wei L, Huang Y, Liu D, Jia Y, Luo C, Lin Y, Liang C, Hu Y, *et al*. 2023. BnIR: A multi-omics database with various tools for *Brassica napus* research and breeding. Molecular Plant **16**, 775–789.

Yang Z, Yang J, Wang Y, Wang F, Mao W, He Q, Xu J, Wu Z, Mao C. 2020. PROTEIN PHOSPHATASE95 regulates phosphate homeostasis by affecting phosphate transporter trafficking in rice. The Plant Cell **32**, 740–757.

Yoo SD, Cho YH, Sheen J. 2007. Arabidopsis mesophyll protoplasts: a versatile cell system for transient gene expression analysis. Nat Protocols **2**, 1565–1572.

Yue W, Ying Y, Wang C, Zhao Y, Dong C, Whelan J, Shou H. 2017. OsNLA1, a RING-type ubiquitin ligase, maintains phosphate homeostasis in *Oryza sativa* via degradation of phosphate transporters. The Plant Journal **90**, 1040–1051.

Zhang F, Chen X, Vitousek P. 2013. Chinese agriculture: An experiment for the world. Nature **497**, 33–35.

Zhang Y, Li TT, Wang LF, Guo JX, Lu KK, Song RF, Zuo JX, Chen HH, Liu WC. 2022a. Abscisic acid facilitates phosphate acquisition through the transcription factor ABA INSENSITIVE5 in Arabidopsis. The Plant Journal **111**, 269–281.

Zhang Y, Wang LF, Han SY, Ren F, Liu WC. 2022b. Sorting Nexin1 negatively modulates phosphate uptake by facilitating Phosphate Transporter1;1 degradation in Arabidopsis. The Plant Journal **111**, 72–84.

Zheng X, Liu C, Qiao L, Zhao J, Han R, Wang X, Ge C, Zhang W, Zhang S, Qiao L, *et al.* 2020. The MYB transcription factor TaPHR3-A1 is involved in phosphate signaling and governs yield-related traits in bread wheat. Journal of Experimental Botany **71**, 5808–5822.

Zhong S, Mahmood K, Bi YM, Rothstein SJ, Ranathunge K. 2017. Altered expression of OsNLA1 modulates Pi accumulation in rice (*oryza sativa* L.) plants. Frontier in Plant Science **8**, 928.

Zhou J, He P, Shan L. 2014. Ubiquitination of plant immune receptors. Methods in Molecular Biology **1209**, 219–231.

Zhou M, Li Y, Lu X, He P, Liang C, Tian J. 2023. Diverse functions of GmNLA1 members in controlling phosphorus homeostasis highlight coordinate response of soybean to nitrogen and phosphorus availability. The Crop Journal **11**, 1251–1260.

Figure & Legends

Figure 1 Expression patterns of *BnaNLA1* genes in *B. napus*. (A) Relative expression of *BnaNLA1* genes in roots and leaves during the period of Pi starvation. Germinated *B. napus* seeds were grown in nutrient solution with sufficient Pi supply (1 mM Pi) for nine days and then transferred to nutrient solutions with low Pi supply (5 μM Pi) for seven days. (B) Relative expression of *BnaNLA1* genes in different tissues at flowering.

Samples were taken from the pot experiment. Data are means (±SD) of three biological replicates. The housekeeping genes *BnaEF1*-α and *BnaTubulin* were used as the internal reference.

Figure 2 GUS staining of *proBnaA09.NLA1::GUS* transgenic *B. napus*. GUS staining: of (A-E) roots, (F-G) cotyledons and three consecutive leaves of *proBnaA09.NLA1::GUS* transgenic *B. napus* under sufficient (+P) and deficient (-P) P supplies. Germinated *proBnaA09NLA1::GUS* transgenic *B. napus* seeds were grown in 1/2 standard Hoagland nutrient solution for 10 days and then transferred to nutrient solutions with 1 mM Pi (+P) and 5 μM Pi (-P) for seven days, respectively. (H-I) GUS staining of the floral organs of *proBnaA09.NLA1::GUS* transgenic *B. napus* at flowering. Samples were taken from the pot experiment. Scale bars: (A) 2 cm, (B, D) 1 mm, (C, E) 2 mm, (F-G) 2 cm, (H) 2 mm and (I) 100 μm.

Figure 3 Regulation of *BnaNLA1s* by *BnamiR827* in roots under P starvation in *B. napus*. (A) Relative expression of *BnamiR827* genes in roots and leaves during a period of Pi deficiency. Germinated *B. napus* seeds were grown in nutrient solution with sufficient Pi supply (1 mM Pi) for nine days and then transferred to nutrient solutions with low Pi supply (5 μM Pi) for seven days. (B) GUS staining of transgenic *Arabidopsis* with *GUS* driven by the promoter of *BnamiR827s*. Transgenic plants were germinated on 1/2 MS medium for five days and then transplanted to 1/2 MS medium with 625 μM Pi (+P) or 6.25 μM Pi (-P) for three days. Scale bars: 200 μm. (C) Relative expression analysis of *BnamiR827s* and *BnaNLA1s* in *BnamiR827* overexpressing lines. 'Westar10' and transgenic plants were grown in nutrient solution with sufficient Pi supply (1 mM Pi) for 16 days and then the roots were sampled. Data are means (±SD) of three biological replicates. Different letters indicate significant differences ($P<0.05$, the Kruskal-Wallis test followed by one-way analysis of variance, Tukey's test).

Figure 4 Subcellular localization of BnaNLA1 proteins in *Arabidopsis* protoplasts. N-terminal GFP fusion constructs were transformed with *Arabidopsis* protoplasts. The

green fluorescence was derived from 35S::GFP-BnaNLA1s. The red fluorescence was derived from 35S::AtPIP2A-mCherry. Scale bars = 10 μm.

Figure 5 *BnaNLA1s* functionally complement *AtNLA1* in the *Arabidopsis nla1* mutant. (A) Shoot growth performance, (B) shoot fresh weight and (C) total chlorophyll concentration of Col-0, *nla1* mutant and 35S::*BnaNLA1*/*nla1* complemented lines under sufficient and deficient nitrate supplies. Data are means (±SD) of three biological replicates. Different letters indicate significant differences within each nitrate treatment ($P<0.05$, the Kruskal-Wallis test followed by one-way analysis of variance, Tukey's test). Scale bars = 3 cm.

Figure 6 Mutation of *BnaNLA1* members and overexpression of *BnamiR827* increase the P accumulation of *B. napus* under both sufficient (+P) and deficient (-P) Pi supplies. (A) The growth phenotype, (B) shoot fresh weight, (C) total root length, (D-E) tissue Pi concentrations and (F-G) tissue P concentrations of *BnaA09.NLA1*/*BnaC08.NLA1* and *BnaA09.NLA1* mutant lines and 'Westar10' under +P and –P supplies. (H) The growth phenotype, (I) shoot fresh weight, (J) total root length, and (K, L) tissue Pi concentrations of the *BnamiR827* overexpressing lines and 'Westar10' under +P and -P supplies, respectively. Data are means (±SD) of three biological replicates. Significant differences compared with 'Westar10' under the same P supply were determined using Student's t-test (* $P < 0.05$, ** $P < 0.01$, *** $P < 0.001$). Scale bars = 2 cm. R, roots; C, cotyledon; L1 to L4, consecutive leaves from the oldest to the youngest; SBR, shoot basal region.

Figure 7 *BnamiR827* and *BnaA09.NLA1* regulates pollen viability in *B. napus*. (A) Pollen viability stained by KI-I_2 solution in 'Westar10', *BnaA09.NLA1*-KO, *BnaA09.NLA1*/*BnaC08.NLA1*-KO, and *BnamiR827*-OE lines. Pollen grains were collected from the flowers of *B. napus*. The black, brown, and yellow or transparent dots indicated fully stained, partially stained, and not stained pollen grains, respectively. Scale bars = 100 μm. (B) The percentage of not stained, partially stained, and fully

stained pollen grains. Data are means ± SD (n=3). Different letters indicate significant differences ($P<0.05$, one-way analysis of variance, Duncan's test). (C) Pi concentrations of stamen, pistil, petal, and sepal in 'Westar10', *BnaA09.NLA1*-KO, *BnaA09.NLA1*/*BnaC08.NLA1*-KO, and *BnamiR827*-OE lines. Data are means ± SD (n=4). All data are plotted with box and whiskers plots. Whiskers plot represents minimum and maximum values, and box plot represents second quartile, median and third quartile. Different letters indicate significant differences among genotypes ($P<0.05$, one-way analysis of variance, Tukey's test).

Figure 8 Growth performance and agronomy index of 'Westar10', *BnaA09.NLA1*-KO, *BnaA09.NLA1*/*BnaC08.NLA1*-KO, and *BnamiR827*-OE lines in the field trial. (A, K) Shoot growth phenotype. (A) Scale bars = 20 cm. (K) Scale bars = 15 cm. (B, L) Seed yield per plant. Scale bars = 2 cm. (C, M) Plant height, (D, N) shoot dry weight, (E, O) shoot P concentration, (F, P) branch numbers, (G, Q) pod numbers per plant, (H, R) seed numbers per pod, (I, S) seed yield per plant, and (J, T) 1000-seed weight of 'Westar10', *BnaA09.NLA1*-KO, *BnaA09.NLA1*/*BnaC08.NLA1*-KO, and *BnamiR827*-OE lines. Data are means ± SD (n=4/6). All data are plotted with box and whiskers plots. Whiskers plot represents minimum and maximum values, and box plot represents second quartile, median and third quartile. Different letters indicate significant differences among genotypes ($P<0.05$, one-way analysis of variance, Duncan's test).

Figure 9 BnaA09.NLA1 ^{C275A} interacts with several BnaPHT1 family Pi transporters. Bimolecular fluorescence complementation (BiFC) analysis to detect the interaction between (A) BnaA09.NLA1 or (B) BnaA09.NLA1^{C275A} and BnaPT8, BnaPT10, BnaPT11, BnaPT27, BnaPT35, BnaPT37 and BnaPT42 in tobacco leaves. N-terminal fragments of YFP (nYFP) were fused to N-terminus of wild-type BnaA09.NLA1 or mutated version of BnaA09.NLA1 (BnaA09.NLA1^{C275A}), and C-terminal fragments of YFP (cYFP) were fused to N-terminus of BnaPHT1s. Scale bars = 10 μm. (C) E3 ubiquitin ligase activities of MBP-AtNLA1 and MBP-AtNLA1^{C279A} in the presence of AtUBA1-His (E1), AtUBC8-His (E2) and ubiquitin-Flag. Anti-Flag antibody was used

to detect ubiquitinated proteins. (D) Split-ubiquitin Y2H assays of BnaA09.NLA1^{C275A} interacts with BnaPHT1s. The pNubG-Fe65 and pTSU2-APP plasmid combination was used as the positive control, while the pPR3-N and pBT3-N-BnaPHT1 plasmids were co-transformed into yeast cells as the negative controls and self-activation controls. The seven experimental groups, i.e., the pPR3-N-BnaA09.NLA1^{C275A} and pBT3-N-BnaPT8 plasmids, the pPR3-N-BnaA09.NLA1^{C275A} and pBT3-N-BnaPT10 plasmids, the pPR3-N-BnaA09.NLA1^{C275A} and pBT3-N-BnaPT11 plasmids, the pPR3-N-BnaA09.NLA1^{C275A} and pBT3-N-BnaPT27 plasmids, the pPR3-N-BnaA09.NLA1^{C275A} and pBT3-N-BnaPT35 plasmids, the pPR3-N-BnaA09.NLA1^{C275A} and pBT3-N-BnaPT37 plasmids, and the pPR3-N-BnaA09.NLA1^{C275A} and pBT3-N-BnaPT42 plasmids, were co-transformed into yeast cells, respectively. Yeast cells were grown in liquid culture and spotted on plates with double dropout medium (SD/−Leu/−Trp, SD-LW), triple dropout medium (SD/−Leu/−Trp/−His, SD-LWH) or quadruple dropout medium (SD/−Leu/−Trp/−His/−Ade, SD-LWHA). Successful plasmid transfection is indicated by positive yeast clones on the double dropout medium plates. The presence of clones on the triple dropout medium plates indicates successful expression of the *His3* reporter gene, while the presence of clones on the quadruple dropout medium indicates successful expression of the *Ade2* reporter gene.

Figure 10 A working model of the *BnamiR827–BnaA09.NLA1–BnaPHT1s* axis in regulating Pi homeostasis, pollen viability and seed yield in *B. napus*. *BnamiR827* induced by P deficiency represses the expression of *BnaNLA1s* in roots at post-transcriptional level, and then BnaA09.NLA1 mediates the degradation of several BnaPHT1s (i.e., BnaPT8, BnaPT10, BnaPT11, BnaPT27, BnaPT35, BnaPT37 and BnaPT42) to regulate Pi uptake, Pi homeostasis in anthers, pollen viability and seed yield in *B. napus*.

Figure 1.

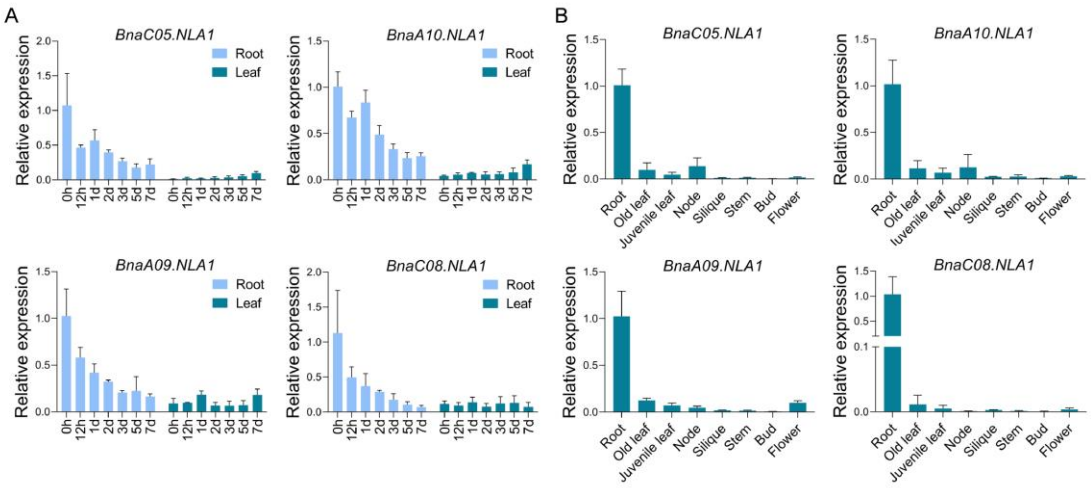
A
B
BnaC05.NLA1
BnaA10.NLA1
BnaA09.NLA1
BnaC08.NLA1
Root
Leaf
Relative expression
0h
12h
1d
2d
3d
5d
7d
Root
Old leaf
Juvenile leaf
Node
Silique
Stem
Bud
Flower

1080 Figure 2.

1081

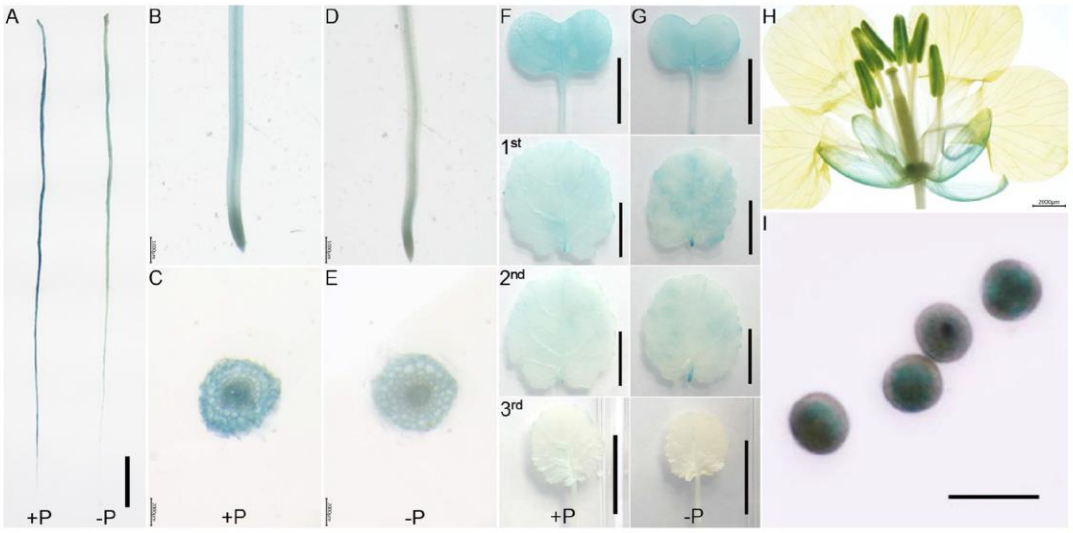

1082

1083

1084 Figure 3

1085

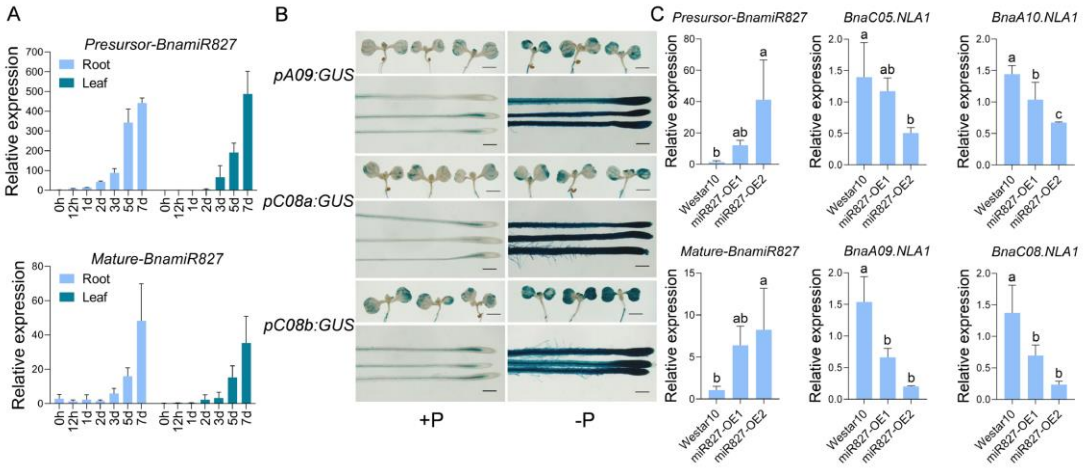

1086

1087

1088

1089 Figure 4

1090

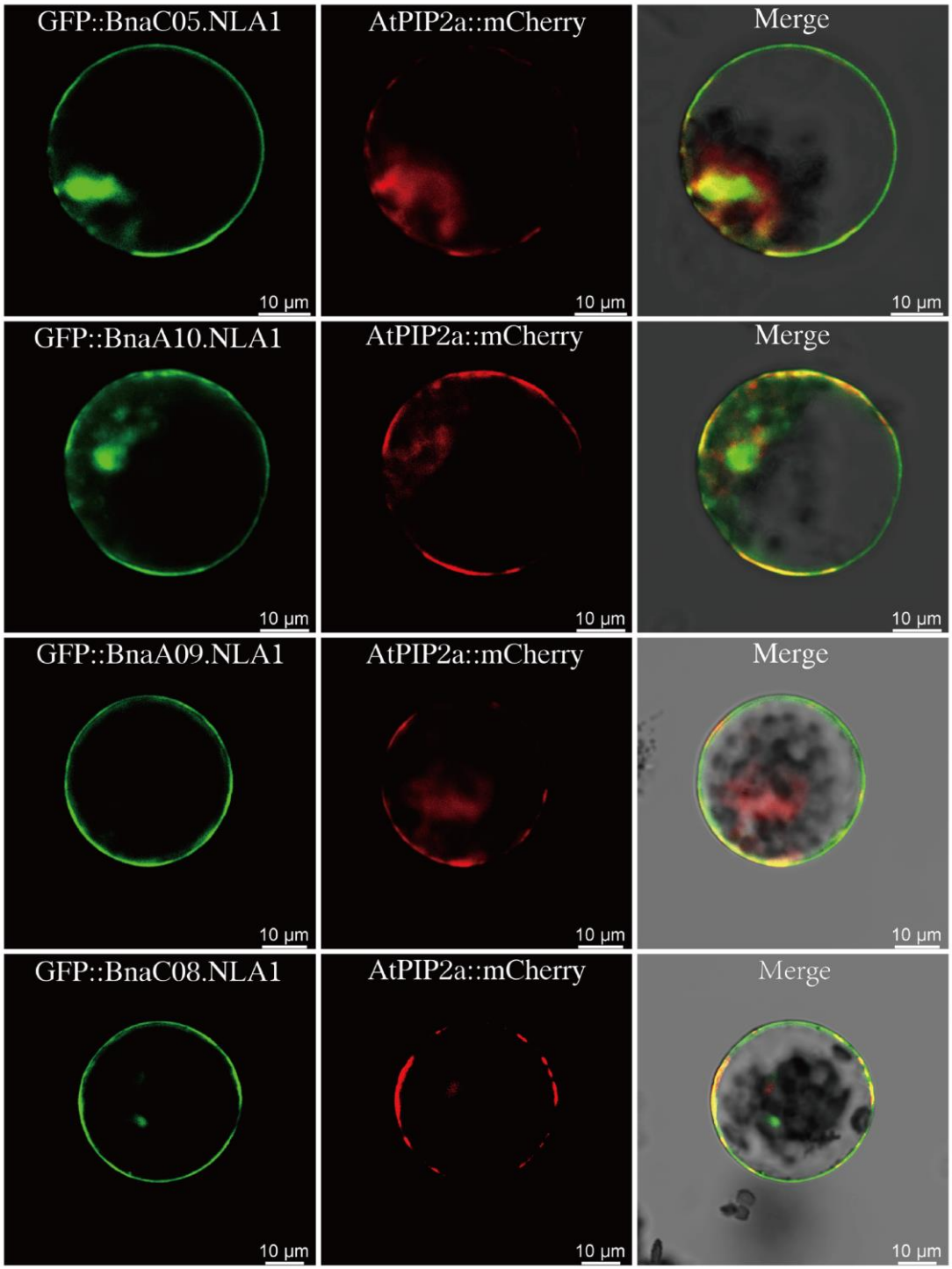

1091

1092

1093 Figure 5

1094

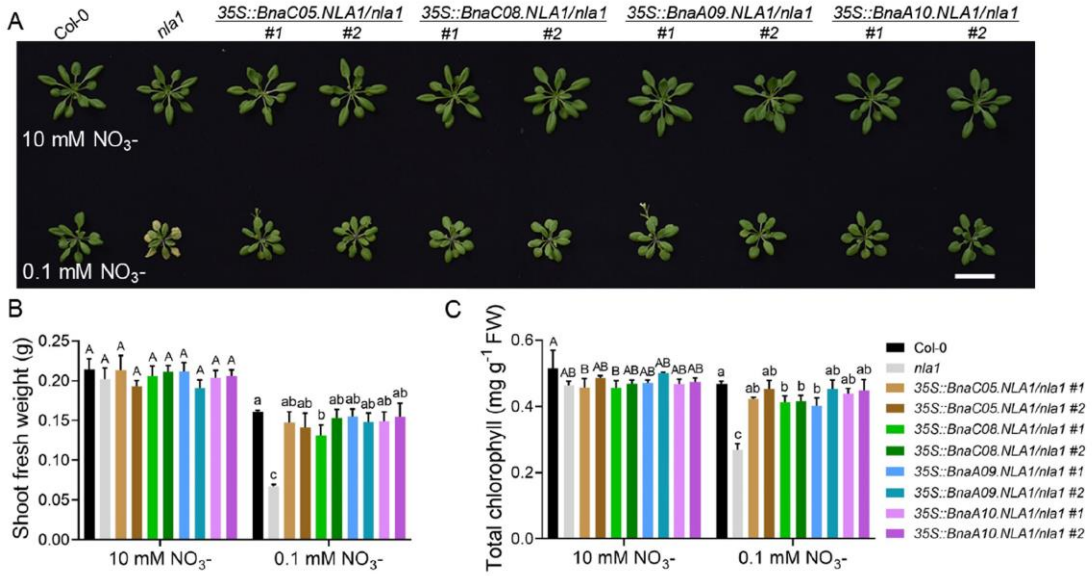

1095

1096

1097

Figure 6

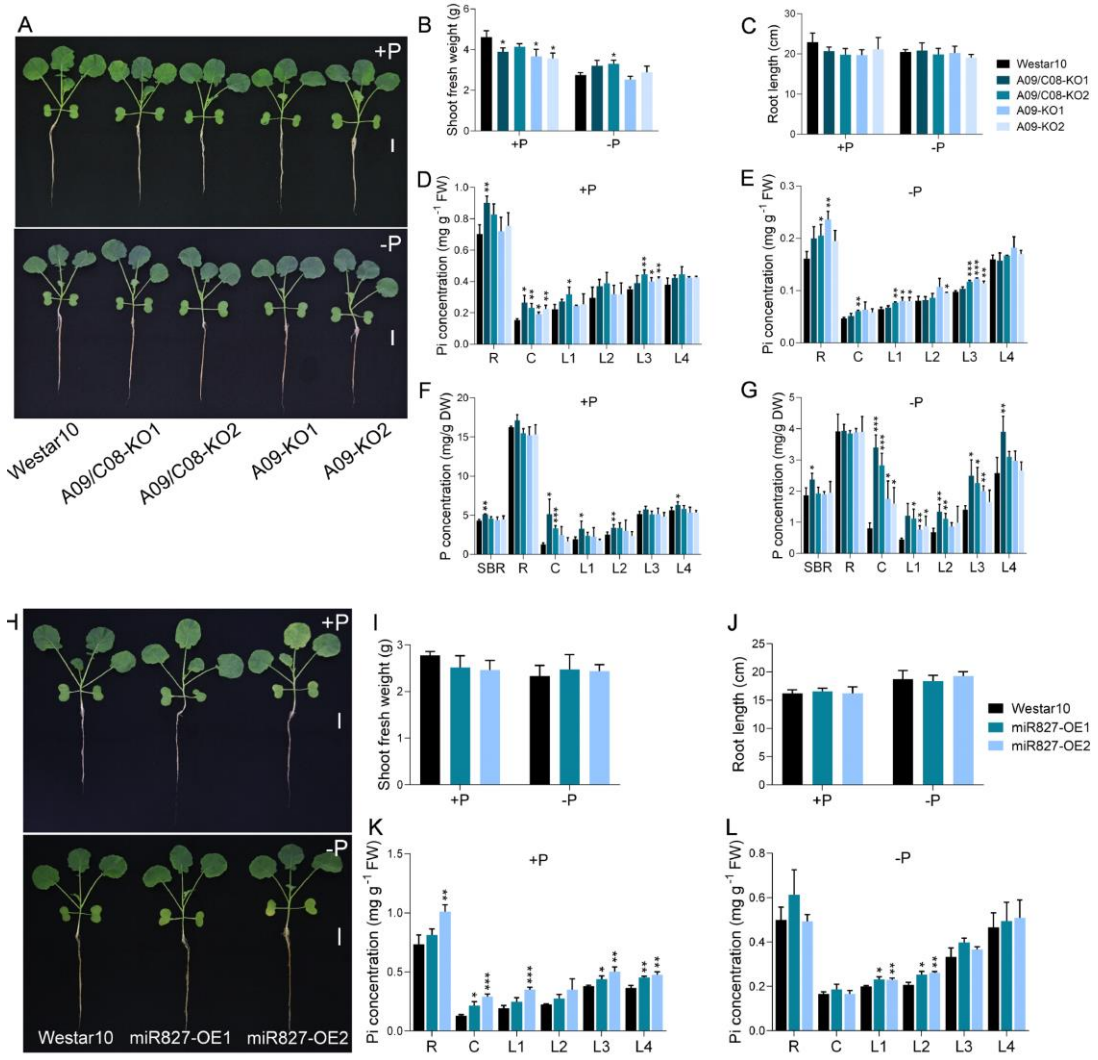
A
+P
-P
Westar10
A09/C08-KO1
A09/C08-KO2
A09-KO1
A09-KO2
B
Shoot fresh weight (g)
+P
-P
C
Root length (cm)
Westar10
A09/C08-KO1
A09/C08-KO2
A09-KO1
A09-KO2
D
+P
Pi concentration (mg g-1 FW)
R C L1 L2 L3 L4
E
-P
Pi concentration (mg g-1 FW)
R C L1 L2 L3 L4
F
+P
P concentration (mg/g DW)
SBR R C L1 L2 L3 L4
G
-P
P concentration (mg/g DW)
SBR R C L1 L2 L3 L4
H
+P
-P
Westar10
miR827-OE1
miR827-OE2
I
Shoot fresh weight (g)
+P
-P
J
Root length (cm)
Westar10
miR827-OE1
miR827-OE2
K
+P
Pi concentration (mg g-1 FW)
R C L1 L2 L3 L4
L
-P
Pi concentration (mg g-1 FW)
R C L1 L2 L3 L4

1103 Figure 7

1104

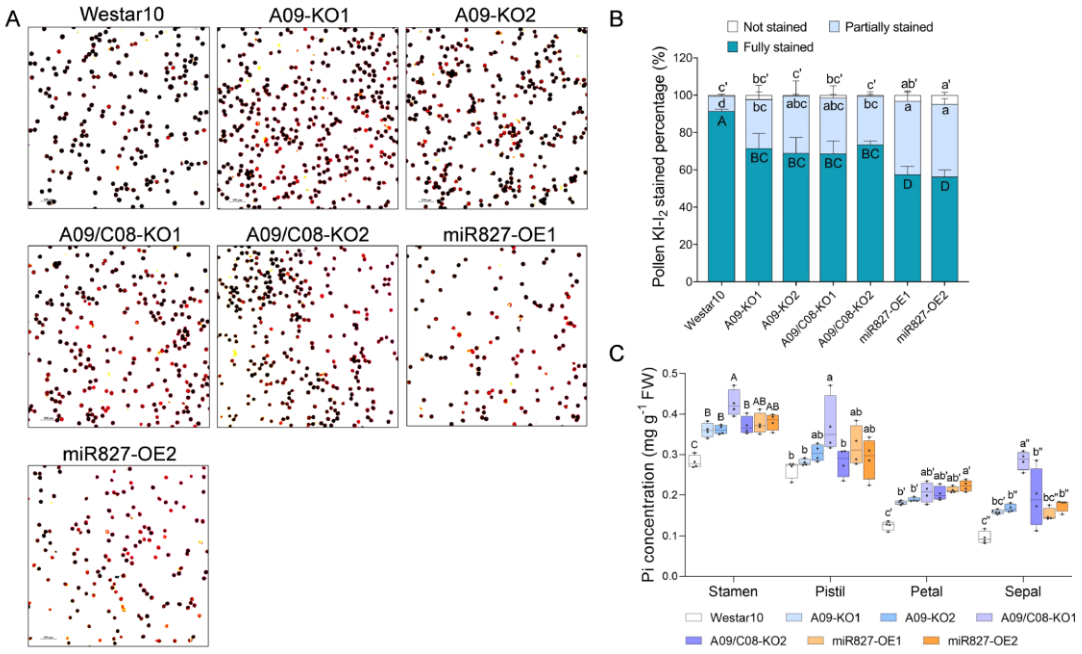

1105

1106

1107

Figure 8

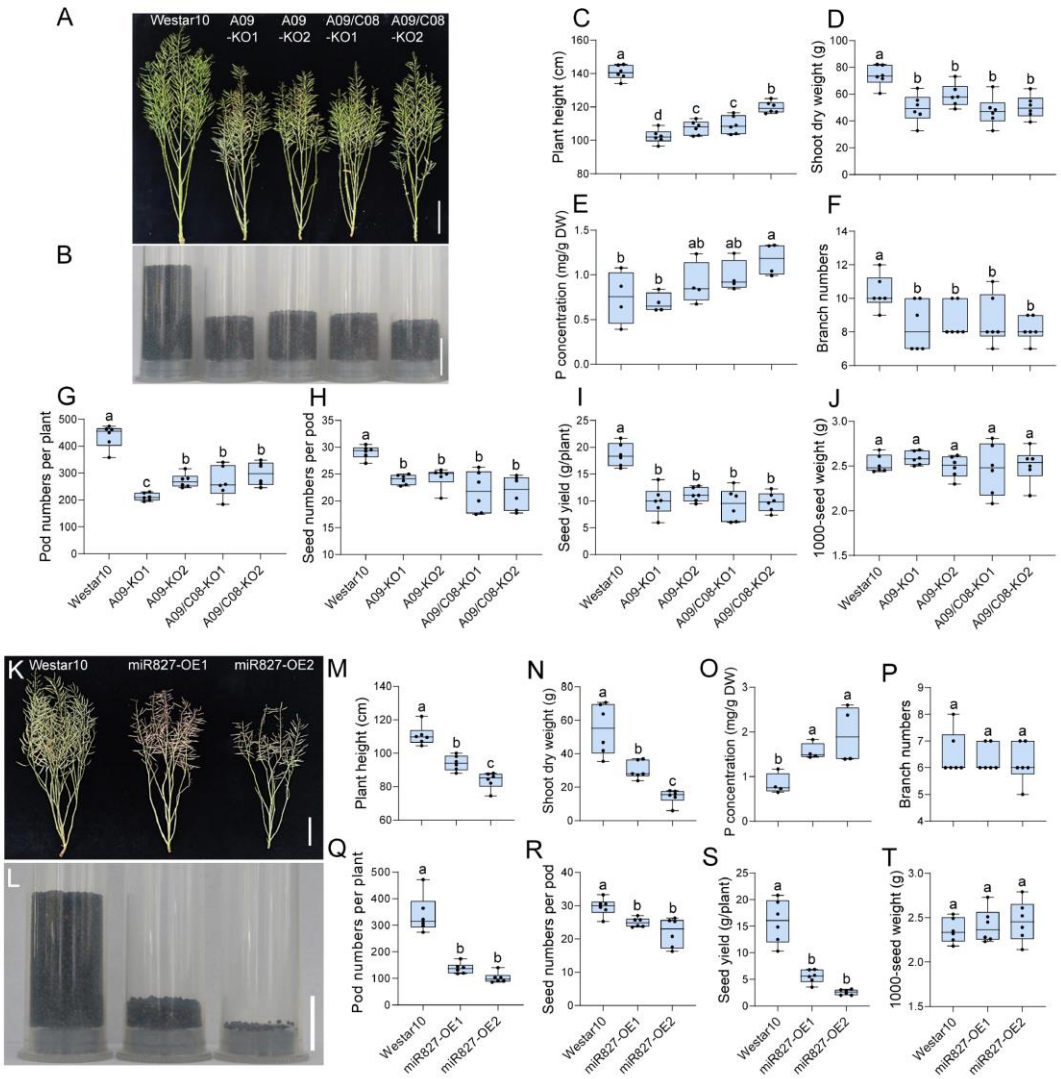
A
Westar10
A09 -KO1
A09 -KO2
A09/C08 -KO1
A09/C08 -KO2
B
C
Plant height (cm)
D
Shoot dry weight (g)
E
P concentration (mg/g DW)
F
Branch numbers
G
Pod numbers per plant
H
Seed numbers per pod
I
Seed yield (g/plant)
J
1000-seed weight (g)
Westar10
A09-KO1
A09-KO2
A09/C08-KO1
A09/C08-KO2
K
Westar10
miR827-OE1
miR827-OE2
L
M
Plant height (cm)
N
Shoot dry weight (g)
O
P concentration (mg/g DW)
P
Branch numbers
Q
Pod numbers per plant
R
Seed numbers per pod
S
Seed yield (g/plant)
T
1000-seed weight (g)
Westar10
miR827-OE1
miR827-OE2

1113 Figure 9

1114

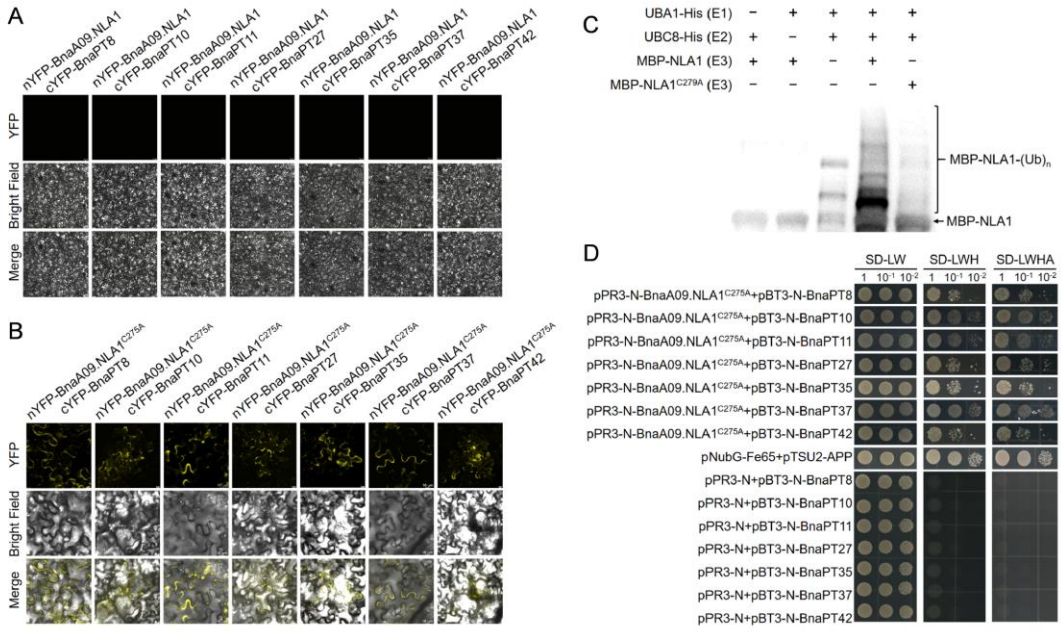

1115

1116

1117

1118 Figure 10

1119

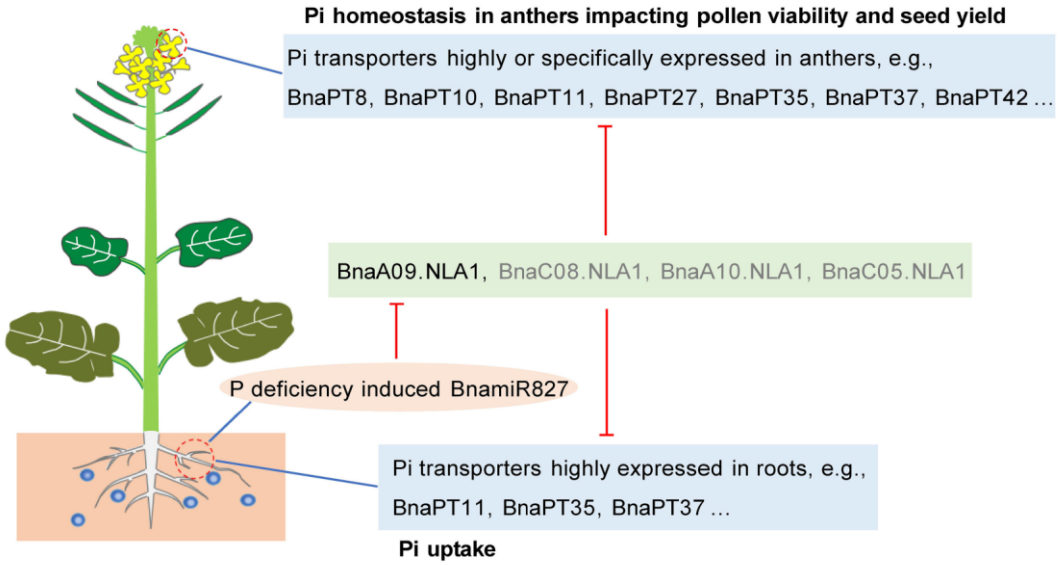

1120